GOCE High Level Processing Facility Technical Note

Release 6 GOCE Gravity Field Models Validation Report

Doc. No.: GO-TN-HPF-GS-0337
Issue: 1
Revision: 0
Date: 30 / 06 / 2019

Prepared by: The European GOCE Gravity Consortium
EGG-C

Document Information Sheet

Document Name
Release 6 GOCE Gravity Field Models Validation Report

Document ID	Issue	Date
GO-TN-HPF-GS-0337	1.0	30.06.2019

Author	Institute
T. Gruber, X. Oikonomidou	IAPG
S. Bruinsma	CNES
P, Visser	TU Delft
S. Mulet	CLS
Contributions from	Institute

Document Category	Document Class	Document Level

Configuration Item		Confidentiality Level

Appropriate Signatures		
Name	signature	Signature for approval

Distribution List	
Person	Institute
HPF Team	
R. Floberghagen	ESA

List	
DIL	NO
CDL	NO
CIDL	NO
CSL	NO
CCN	NO
SWPRL	NO

Data Package	
SRR	NO
ADIR	NO
CDR	NO
AR0	NO
AR 1	NO
AR 2	NO

Table of Contents

1. INTRODUCTION

This technical note summarizes the validation results for the release 6 GOCE gravity field models. Validation is performed in different ways, namely

- by analysing the signals and errors of the models compared to previous releases,
- by computing MDT solution based on the release 6 gravity fields and comparing them with in-situ drifter data,
- by comparing model derived geoid heights with independent geoid information at GNSS-levelling stations, and
- by computing orbits using the release 6 gravity field models for various satellites.

Table 1-1summarizes the GOCE release 6 gravity field models which are validated by these techniques in the subsequent sections.

Table 1-1: Summary of Release 6 GOCE models under validation

Short Name	**Long Name & Description**
DIR6	GO_CONS_EGM_GOC_2__20091009T000000_20131020T235959_0201 (Förste et al, 2019) GOCE Input Data: - Gradients: EGG_NOM_2 (re-calibrated release 2018) - Orbits: SST_PRD_2 (reduced dynamic orbits) - Attitude: EGG_IAQ_2C - Data period: 20091009T000000-20131020T235959 A-priori Information used: The a-priori gravity field for the processing of the GOCE gravity gradients was the GOCE-model 5th release from the direct approach GO_CONS_GCF_2_DIR_R5 up to its maximum degree/order 300 (Bruinsma et al. 2014). Processing Procedures: The GOCE gravity gradients were processed without applying the external calibration corrections. The observation equations were filtered with a 0 - 125.0 mHz lowpass filter. Subsequently "SGG" normal equations to degree/order 300 have been computed separately for 46 continuous time segments of approximately 1270 days totally (identified after the preprocessing of the data) and for each of the gradient components Txx, Tyy, Tzz and Txz. The Txx, Tyy, Tzz and Txz SGG normal equations were accumulated with the relative weight 1.0. But within the SGG components, all observation equations have been weighted individually according to its standard deviation estimated w.r.t. the a-priori gravity field. To overcome the numerical instability of the GOCE-SGG normal equation due to the polar gaps and to compensate for the poor sensitivity of the GOCE measurements in the low orders the following stabilizations were applied: 1) The GOCE-SGG normal equation was fully combined with GRACE and SLR normal equations. 2) A spherical cap regularization in accordance to Metzler and Pail (2005) was iteratively computed to d/o 300 using the GRACE/SLR data mentioned below to degree/order 130. 3) Additionally a Kaula regularization was applied to all coefficients beyond degree 180 The solution was obtained by Cholesky decomposition of the accumulated normal equations. Details of the GRACE contribution: The GRACE part consists of 85 monthly normal equations to degree/order 200 out of the time span January 2007 till November 2014 from GFZ's GRACE Release 06 processing based on GNSS-SST and K-Band-Range-Rate data. For details of this GRACE release see Dahle et al. 2018. Very low Degrees: The harmonics of very-low degree, in particular degrees 2 and 3, cannot be estimated accurately with GRACE and GOCE data only. Therefore, normal equations from the following SLR missions were used in the combination in order to improve the gravity field solution: LAGEOS-1/2, AJISAI,

	STARLETTE and STELLA from Jan. 2002 till Oct. 2018, LARES from Feb. 2012 till Oct. 2018; The SLR tracking data were processed according to the GRACE Release 6 standards Combination: During the combination with GOCE, the GRACE contribution was taken only up to degree/order 130 and the SLR contribution only up to degree/oder 5. As GRACE is sensitive for temporal variations in the Earth gravity field, the date 20100901 should be taken as reference epoch of this model. This date is mean of the included GRACE measurement time span by considering the mentioned missed months. This reference epoch is close to the mean of the measurement time span of the included SLR tracking data (20100701) Specific features of resulting gravity field The model is a satellite-only model based on a full combination of GOCE-SGG with GRACE and SLR tracking data, leading to both excellent orbit fits as well as GPS/levelling results. Processing details are presented in Bruinsma et al. 2010 and Pail et al. 2011.
TIM6	GO_CONS_EGM_GOC_2__20091009T000000_20131021T000000_0201 (Brockmann et al, 2019) GOCE Input Data: - Gradients: EGG_NOM_2 (re-calibration, released 2018, version 0202) - Orbits: SST_PKI (kinematic orbits); SST_PCV (variance information of kinematic orbit positions), SST_RNX (original RINEX orbit data) - Attitude: EGG_IAQ_2C - Non-conservative accelerations: EGG_CCD_2C - Data period: 09/10/2009 - 20/10/2013 No static a-priori gravity field information applied (neither as reference model, nor for constraining the solution) Processing procedures: Gravity from orbits (SST): Short-arc integral method applied to kinematic orbits, up to degree/order 150; Orbit variance information included as part of the stochastic model, it is refined by empirical covariance functions Gravity from gradients (SGG): Parameterization up to degree/order 300; Observations used: Vxx, Vyy, Vzz and Vxz in the Gradiometer Reference Frame (GRF); Realistic stochastic modelling by applying digital decorrelation filters to the observation equations; estimated separately for individual data segments applying a robust procedure. Combined solution: Addition of normal equations (SST D/O 150, SGG D/O 300); Constraints: Kaula-regularization applied to coefficients of degrees/orders 201 - 300 (constrained towards zero); Observation equations for zero gravity anomaly observations in polar regions (>83°) to constrain polar gaps towards zero (degree 11 to 300); Optimum weighting (SST, SGG, constraints) based on variance component estimation. Specific features of resulting gravity field: Gravity field solution is independent of any other gravity field information; Constraint towards zero starting from degree/order 201 to improve signal-to-noise ratio; Related variance-covariance information represents very well the true errors of the coefficients; Solution can be used for independent comparison and combination on normal equation level with other satellite-only models (e.g. GRACE), terrestrial gravity data, and altimetry ; Since in the low degrees the solution is based solely on GOCE orbits, it is not competitive with a GRACE model in this spectral region
TIM6e	GO_CONS_EGM_GOC_2__20091009T000000_20160119T235959_0201 (Zingerle et al, 2019) Short description: TIM6e is an extended version of the satellity-only global gravity field model TIM6, which includes additional terrestrial gravity field observations over GOCE's polar gap areas. The included terrestrial information consists of the PolarGap campaign data augumented by the AntGG gravity data compilation over the southern polar gap (>83°S) and the ArcGP data over the northern polar gap (>83°N). Processing procedures: The combination is performed on normal equation level, encompassing the terrestrial data as spectrally limited geographic 0.5°x0.5° grids over the polar gaps. Gravity from orbits (SST): (identical to TIM6) Gravity from gradients (SGG): (identical to TIM6) Gravity from terrestrial observations (TER): Collocation of the original terrestrial data sources onto

	30'x30' geographic gravity disturbance grids (in the polar gap areas above 83° southern/northern latitude, thus forming a pair of polar caps); Spectral limitation of the data to D/O 300 within the collocation process; The chosen grid is fully compatible with the grid of the zero observation constraints of the original TIM6 model. In its function it replaces the original constraints from the collocated polar caps, a partial normal equation system, up to d/o 300 is derived. Combined solution: Addition of normal equations (SST D/O 150, SGG D/O 300, TER D/O 300); Constraints: Kaula-regularization applied to coefficients of degrees/orders 201 - 300 (constrained towards zero, fully compatible with TIM6); Weighting of SST and SGG is identical to TIM6. All TER observations are weighted with 5 mGal. Specific features of resulting gravity field: Gravity field solution is (mostly) independent of any other gravity field information (outside the polar gap region); Constraint towards zero starting from degree/order 201 to improve signal-to-noise ratio; Related variance-covariance information represents very well the true errors of the coefficients (outside the polar gap region); Solution can be used for independent comparison and combination on normal equation level with other satellite-only models (e.g. GRACE).

Please note that the TIM6e model is only validated by means of geoid error and orbit computations, as this model is quasi identical to the TIM6 model in the latitude band covered by the GOCE mission (±83.5 degree latitude). The reason is, that in the non-covered areas by GOCE there are no independent comparison data available, and that the signal content is similar to the TIM6 model as this forms the basis of the TIM6e model.

2. SIGNAL AND ERROR ANALYSIS OF REL.6 MODELS

2.1 SIGNAL ANALYSIS

As a first analysis it shall be identified how the signal content of the rel. 6 GOCE models compare to the previous solutions. As a simple tool to investigate this, signal degree variances of the GOCE models and signal degree variances of differences to a high resolution global model incorporating terrestrial and altimetric data are analyzed. Figure 2-1 left shows the square root of the signal degree variances in terms of geoid heights for a selected spectral range from degree 150 to degree 250. It clearly can be identified that with each release of the GOCE models the signal strength became higher meaning that the models are closer to the combined XGM2016 model which is also based on GOCE rel. 5 and terrestrial and altimetric gravity information. In some sense the XGM2016 model represents the true signal strength of the Earth gravity field. It is remarkable that the rel. 6 models (red and dark blue) even contain more signal than the rel. 5 models which is a clear indicator that the reprocessed GOCE gradients contain more and better information.

Figure 2-1 right only shows the rel. 6 GOCE models and the XGM2016 model for the spectral band between degree 180 and 280. One can identify that both rel. 6 models have similar signal strength in this range and that starting between degree 205 and 220 the GOCE rel. 6 models start to loose signal compared to the XGM2016 model. This tells us that in a global average the GOCE rel. 6 models contain the full signal of the Earth gravity field up to this resolution (which is below 100 km corresponding to degree 200).

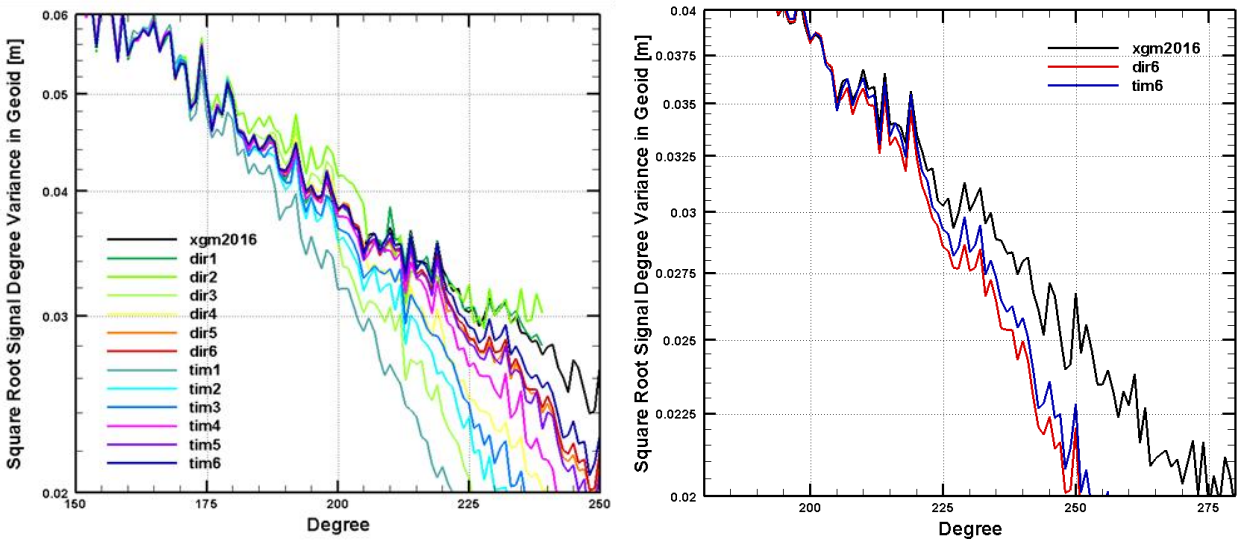

Figure 2-1: Left: Signal degree variances (square root) of DIR and TIM models (rel.1 to rel.6); Right: Signal degree variances (square root) of DIR6 and TIM6 models between degree 180 and 280.

Another interesting approach to evaluate the signal content of the GOCE models is to compare them to the XGM2016 model and to plot signal differences degree variances. These are shown in Figure 2-2 in terms of differences per degree (left) and in terms of accumulated differences (right). First of all one can identify the impact of the polar gap on the TIM

solutions as they do not use other information than from GOCE. The zig zag pattern of the differences shows the weakness of the zonal and near zonal coefficients in these models, which cannot determined without applying regularizations (constraints). For the rel. 6 TIM model it can be seen that the pattern is much smaller. The reason behind this is that stronger constraints by adding zero observations over the polar areas have been applied. The bulk visible for the TIM model differences to XGM2016 is caused by the less good information for the lower degrees, which in contrast are covered by the GRACE information included to the DIR models. When accumulating the differences to XGM2016 one get some initial idea about the differences of the GOCE models to the combined XGM2016 model. DIR models in general show smaller differences due to the GRACE data (see above). But it is also visible that the rel. 6 models in both cases are closest to the XGM2016 model what tells us again that they contain more signal. For example, at degree 200 the average difference of the DIR rel. 6 model to XGM2016 is at a level of 2 cm and at a level of 3.5 cm for the TIM rel. 6 model. Please note this is a global average also including the polar gap areas where no information is provided by GOCE. In the GOCE covered areas the differences are significantly smaller. More details are shown in section 4 where comparisons to observed geoid heights over land are shown.

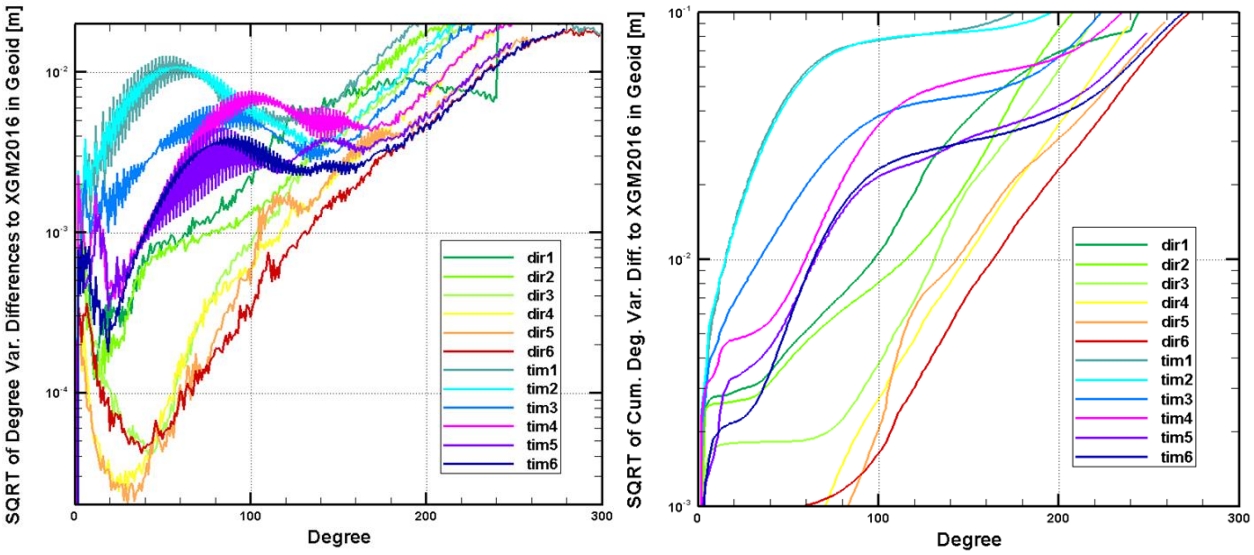

Figure 2-2: Left: Differences of signal degree variances to the XGM2016 model; Right: Cumulative signal degree variance differences to XGM2016 model (square root)

2.2 ERROR ANALYSIS

In order to assess global gravity field models the estimated errors also provide valuable information to get a complete view about their quality. Figure 2-3 and Figure 2-4 show the triangles of the estimated errors for all DIR and TIM models from rel. 1 to rel. 6. Regarding the DIR models (Figure 2-3) it shall be noted that DIR rel. 1 model included some kind of terrestrial information and therefore this model behaves somehow different and will not be discussed further. Comparing the coefficient errors for the rel. 2 to the rel. 5 models one can clearly see the continuous reduction of the estimated errors, which is mostly due to the data volume. The rel. 6 DIR model shows a slightly higher error level compared to the rel. 5

model, which is caused by an updated weighting scheme of the gravity gradients and the GRACE contribution. In any case it needs to be mentioned that these are estimated errors and that they not necessarily reflect the real errors. More important is the relative behaviour between different groups of degrees and orders.

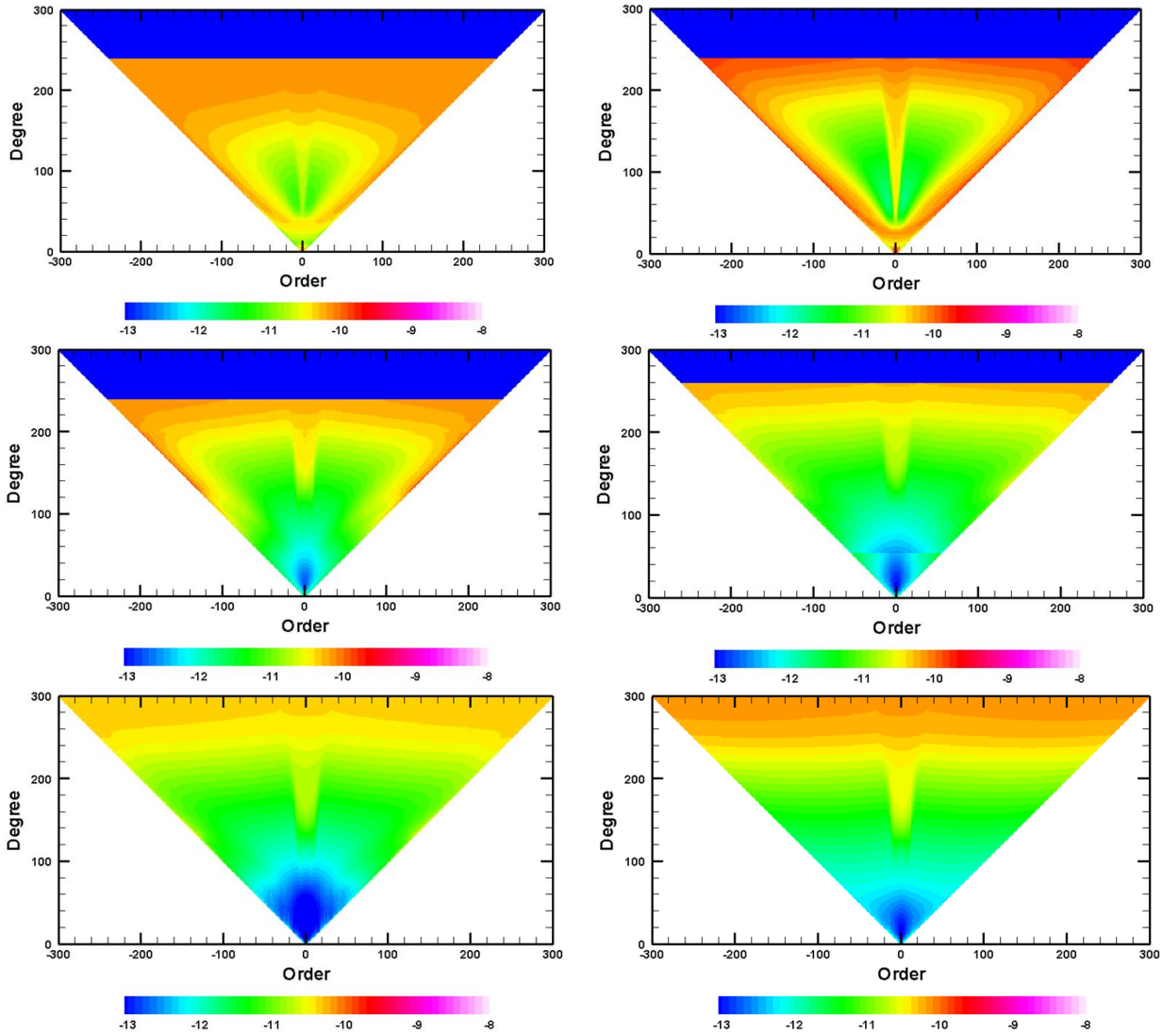

Figure 2-3: Coefficient errors of GOCE DIR models in log10(σC_{nm} and σS_{nm}); σC_{nm} are shown with positive orders, σS_{nm} are plotted with negative orders. Row 1: DIR1 and DIR2 (left, right); Row 2: DIR3 and DIR4; Row 3: DIR5 and DIR6.

Regarding the coefficient errors of the TIM releases (Figure 2-4) some differences to the DIR models become obvious. First of all the zonal and near zonal coefficients exhibit a much larger error level than other coefficients. This is caused by the polar gap of GOCE, which is compensated by the GRACE data in the DIR models (therefore this is less visible in the DIR models and only for the higher degrees and orders where no GRACE information is entering). It is remarkable that the error level of the zonal and near zonal coefficients of the rel. 6 TIM model is significantly lower than for all other releases. This is due to an updated regularization scheme, which was applied for this model (refer to Table 1-1). Main reason is that zero observations were added to the normal equations system. Apart from this one can

identify the steady reduction of the errors with adding more and more data. In general the error structures of both model series look reasonable.

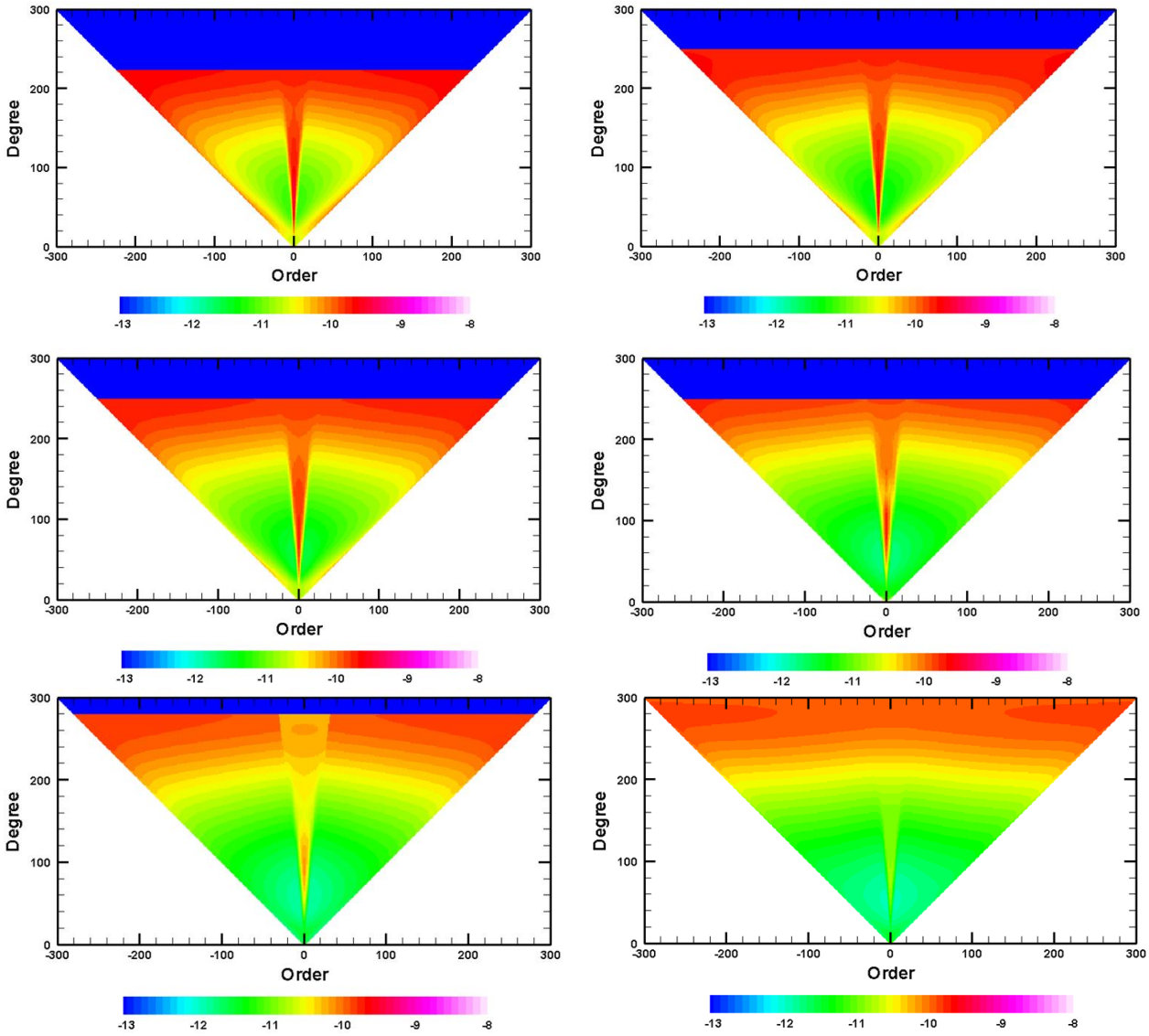

Figure 2-4: Coefficient errors of GOCE TIM models in log10(σC_{nm} and σS_{nm}); σC_{nm} are shown with positive orders, σS_{nm} are plotted with negative orders. Row 1: TIM1 and TIM2 (left, right); Row 2: TIM3 and TIM4; Row 3: TIM5 and TIM6.

In order to estimate the average error of the models, error degree variances in terms of geoid heights (square root) and cumulative geoid height errors are computed (see Figure 2-5). From both plots one can identify the reduction of errors with higher releases (with the exception of DIR6 versus DIR5, which is discussed above). Also the reduction of the errors of the zonal and near zonal coefficients is well visible for the TIM models. For the TIM rel. 6 model the errors do not exhibit anymore the zig-zag and bulky structure which is caused by these coefficient groups. With the cumulative geoid errors one also can nicely estimate the global average error for a specific resolution. E.g. regarding degree 200, which corresponds to a spatial resolution of 100 km, the DIR model series provides the following mean geoid errors

from rel.1 to rel. 6: 6.0 cm, 5.3 cm, 3.2 cm, 1.3 cm, 0.8 cm, 1.0 cm. For the TIM model series the errors at 100 km resolution are from rel. 1 to rel. 6: 10.0 cm, 8.0 cm, 6.0 cm, 4.0 cm, 2.3 cm, 1.6 cm. Both series provide different levels of error estimates, which need to be checked against independent observations in order to identify how good they reflect the true errors. This will be done later in section 4.

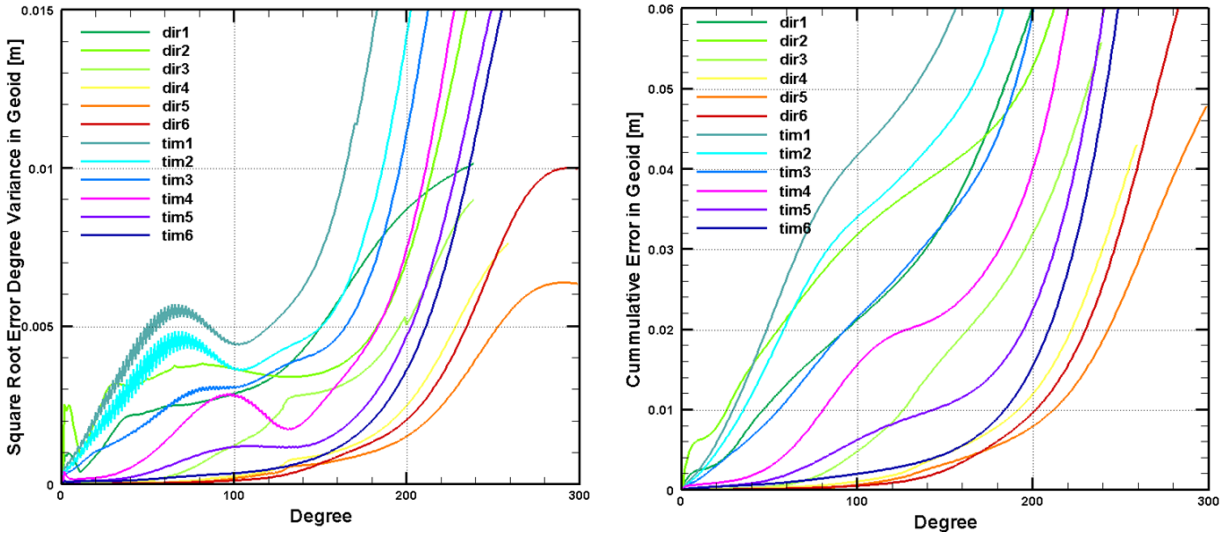

Figure 2-5: Error degree variances (square root) in terms of geoid heights for DIR and TIM gravity field models. Left: per degree; Right: accumulated up to degree.

Finally the full variance-covariance matrix is propagated to the geoid variances in order to show their spatial distribution. Figure 2-6 to Figure 2-8 show the geoid error maps (square root of geoid variances) for the rel. 6 DIR, the rel. 6 TIM and the extended TIM6e model.

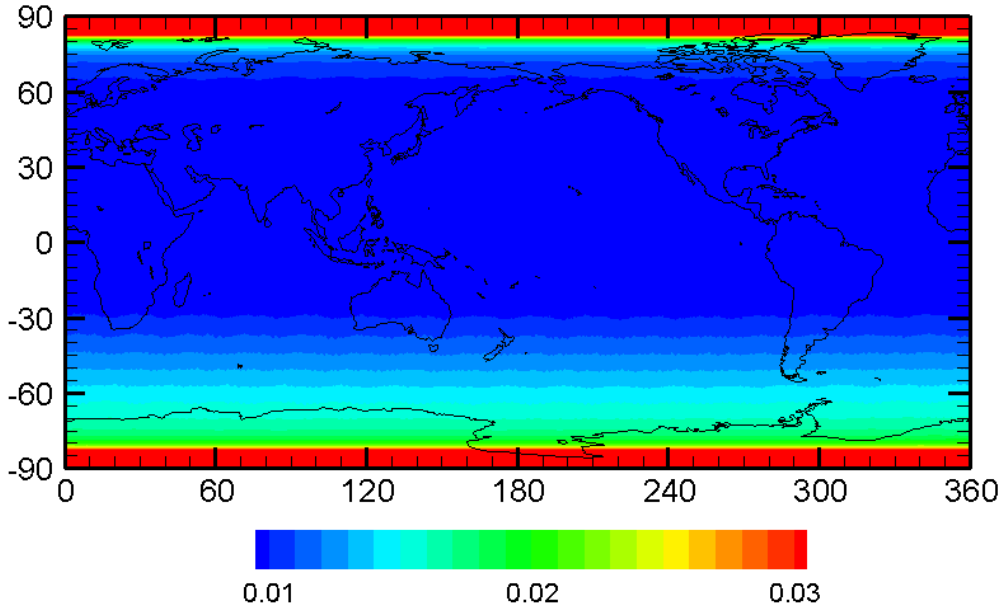

Figure 2-6: Geoid height errors (standard deviation) propagated from the DIR6 variance-covariance matrix [m]

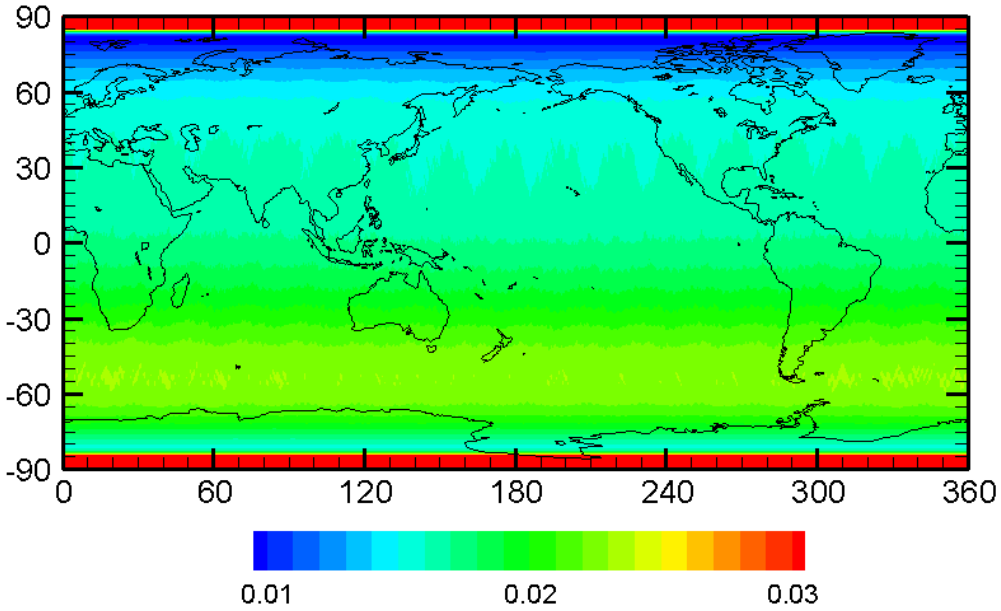

Figure 2-7: Geoid height errors (standard deviation) propagated from the TIM6 variance-covariance matrix [m]

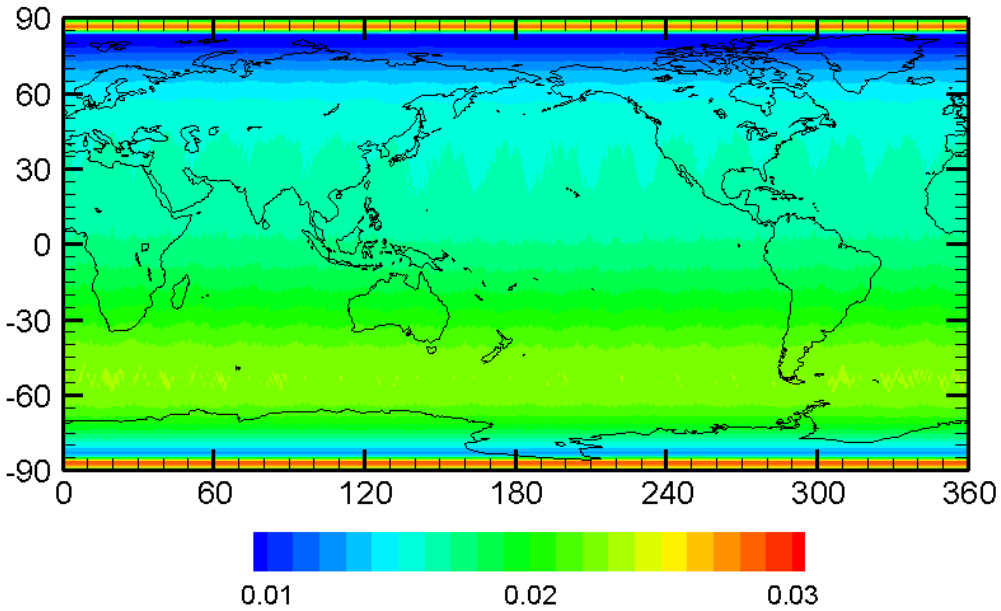

Figure 2-8: Geoid height errors (standard deviation) propagated from the TIM6e variance-covariance matrix [m]

From the geoid error maps one can identify that the estimated error s of the DIR6 model are lower than those from the TIM6 and TIM6e models. This already was visible in coefficient errors and the error degree variances shown in Figure 2-3, Figure 2-4 and Figure 2-5. Disregarding the general error level it is also visible that the structure of the geoid error grids for all models is the same, meaning that there is a slightly higher geoid error in the Southern hemisphere than in the Northern hemisphere and that the geoid errors significantly increase towards the polar gap of GOCE. The first is caused by a small eccentricity of the GOCE orbit leading to slightly lower satellite altitudes in the Northern hemisphere and therefore higher

sensitivity of the GOCE gradiometer. The second observation obviously is caused by missing observation and constraints applied to the DIR6 and TIM6 models. For the TIM6e model it can be identified that the errors in the polar areas are significantly lower, because for this model airborne, terrestrial and altimetric gravity information was included in the polar areas as additional data source and constraints.

2.3 SIGNAL VERSUS ERRORS

Figure 2-9 and Figure 2-10 show the signal to error ratios for the DIR and TIM model series. The numbers shown in both figures indicate the number of significant digits for each coefficient of the spherical harmonic series. The results for both model series confirm the findings shown in the previous chapters. With more data the errors decrease and more coefficients (with higher degrees) can be estimated with a signal to noise ratio higher than 1. From this it can be concluded that the rel. 6 models represent the ultimate solutions with highest possible signal and lowest error levels. As pointed out before, these results heavily rely on realistic estimated errors, which need to be assessed by additional analyses comparing the estimated errors with true errors when comparing the signals to independent observations (see section 4).

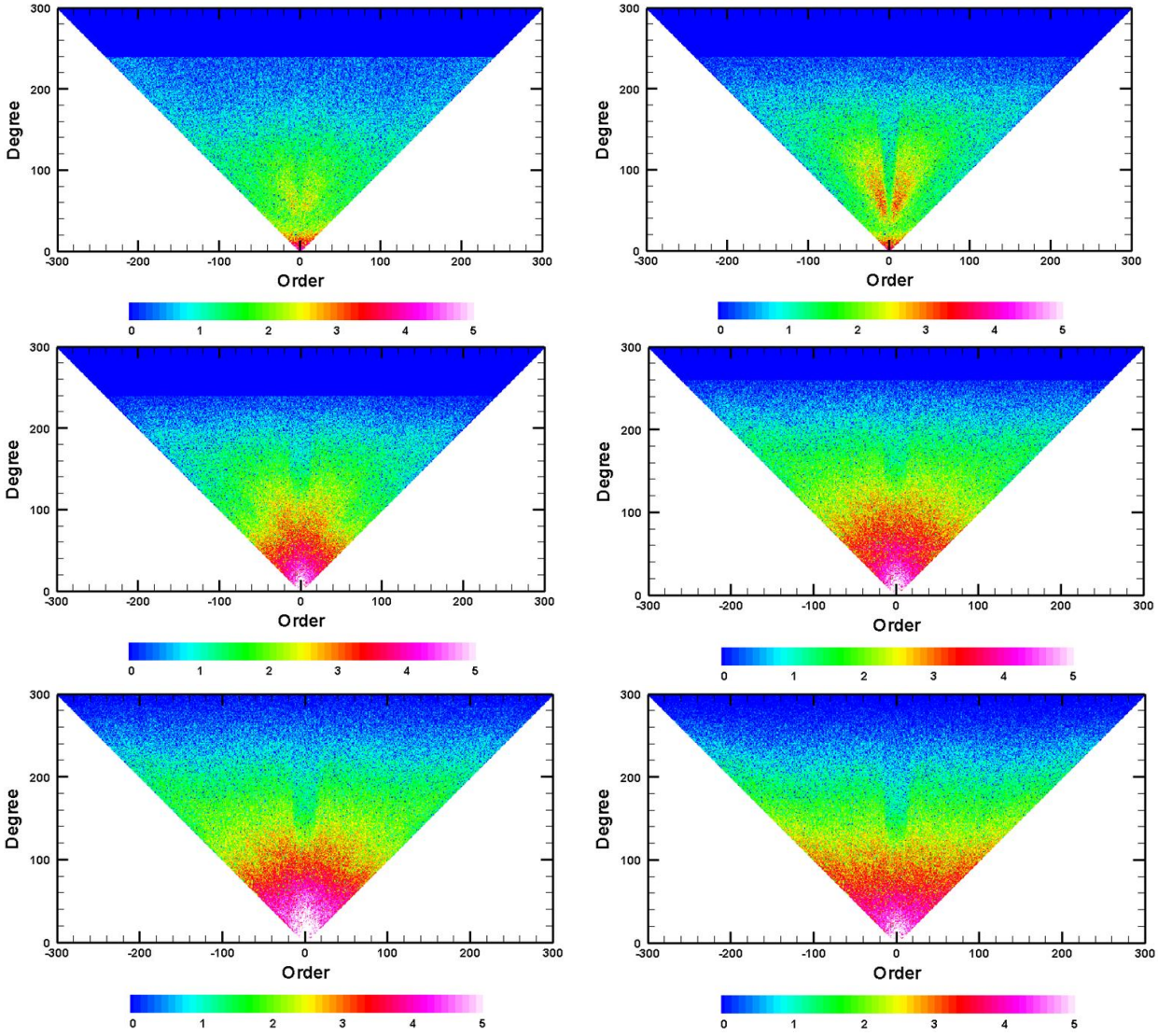

Figure 2-9: Signal to noise ratio of GOCE DIR models in $\log10(C_{nm}/\sigma C_{nm})$ and $\log10(S_{nm}/\sigma S_{nm})$; The numbers indicate the number of significant digits for all coefficients; C-coefficients are shown with positive orders, S-coefficients are plotted with negative orders. Row 1: DIR1 and DIR2 (left, right); Row 2: DIR3 and DIR4; Row 3: DIR5 and DIR6.

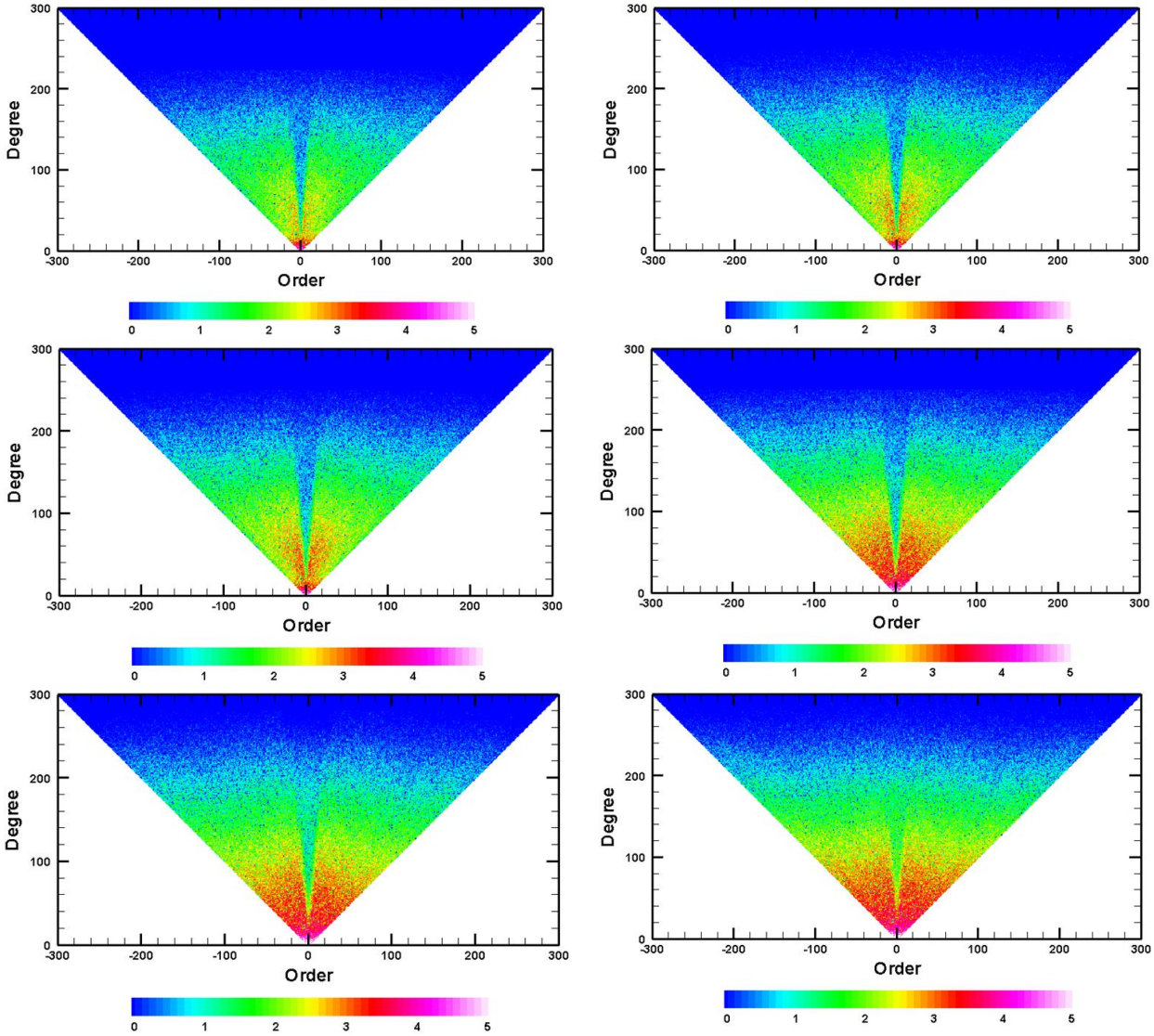

Figure 2-10: Signal to noise ratio of GOCE TIM models in $\log10(C_{nm}/\sigma C_{nm})$ and $\log10(S_{nm}/\sigma S_{nm})$; The numbers indicate the number of significant digits for all coefficients; C-coefficients are shown with positive orders, S-coefficients are plotted with negative orders. Row 1: TIM1 and TIM2 (left, right); Row 2: TIM3 and TIM4; Row 3: TIM5 and TIM6

3. OCEANOGRAPHIC ASSESSMENT OF REL. 6 MODELS

3.1 METHOD

In this study, different geoid models (Table 3-1) are assessed through the computation of geodetic Mean Dynamic Topographies (MDTs). The MDT is computed as the difference between the geoid model and the Mean Sea Surface (MSS) CNES-CLS15 (Pujol et al., 2018). MSS and geoid height are orders of magnitude higher (~100m) than the MDT (~1m), thus the geodetic MDT is very sensitive to geoid model error (and also MSS error).

The assessment method is the following:

1. Computation of geodetic MDT as the difference from MSS CNES-CLS15. The MDTs are filtered at different scales with a Gaussian filter to assess geoid model at different wavelengths.
2. Derivation of associated mean geostrophic currents that are computed from MDT gradients. Equation (1)

$$U_g = -\frac{g}{f}\frac{\partial MDT}{\partial y} \quad ; \quad V_g = \frac{g}{f}\frac{\partial MDT}{\partial x} \tag{1}$$

3. Comparison with independent velocity estimated from drifters (see next section) processed such that they have the same physical content as mean geostrophic currents estimated from geodetic MDT.

Table 3-1: List of tested geoid models

Geoid Models
ITG-Grace
EGM2008
DIR3
DIR4
TIM5
DIR5
TIM6
DIR6

3.2 REFERENCE DATA SET (DRIFTERS)

3.2.1 Processing to Compute Mean Geostrophic Current

As explained in the previous section, the mean geostrophic currents computed from geodetic MDTs are compared with independent estimates from drifters. We use all the 15-meter drogued and undrogued drifting buoy data collected from January 1993 to December 2015 in the framework of the international Surface Velocity Program (SVP). These data are distributed by AOML where they first have been quality controlled and krigged (Hansen and Poulain, 1996) in order to provide 6-hourly velocity measurements. In order to extract from

the drifting buoy velocities only the geostrophic component, the wind driven current (Ekman and Stockes) was first modelled (Rio and Hernandez, 2003 ; Rio et al., 2014) and subtracted. Also, for the undrogued buoys, the wind slippage is estimated (Rio et al., 2014) and subtracted. Then, a 3 day low pass filter is applied to the velocities to remove residual high frequency anti geostrophic currents (inertial and tidal currents). Finally the geostrophic velocity anomalies deduced from the Sea Level Anomalies from CMEMS/DUACS (Pujol et al., 2014) relative to the 1993 - 2012 period are interpolated along the drifters' trajectories and subtracted from the associated instantaneous geostrophic currents to have an estimate of the mean geostrophic currents relative to the same 20-years period. These observations are then averaged in ¼° boxes to reduce residual errors and to end up with "super observations".

3.2.2 Errors of Mean Geostrophic Current Estimated from Drifters

In order to estimate the error of this reference dataset, we also compute 2 additional datasets: one computed only with 15-meter drogued buoys and another computed only with undrogued buoys. Assuming that the two dataset have the same error ε then the mean geostrophic velocity estimated from drogued buoys (U_d) and the mean geostrophic velocities estimated from undrogued buoys (U_{und}) are given by:

$$U_d = U \pm \varepsilon \quad \text{and} \quad U_{und} = U \pm \varepsilon$$

The root mean square of the difference (RMSD) between these two dataset is estimated as follow:

$$RMSD^2 = \frac{1}{N}\sum\left(U_d - U_{und}\right)^2 = \frac{1}{N}\sum\left(2\varepsilon\right)^2 = \left(2\varepsilon\right)^2 \qquad (2)$$

The error is thus given by RMSD/2 (Figure 3-1)

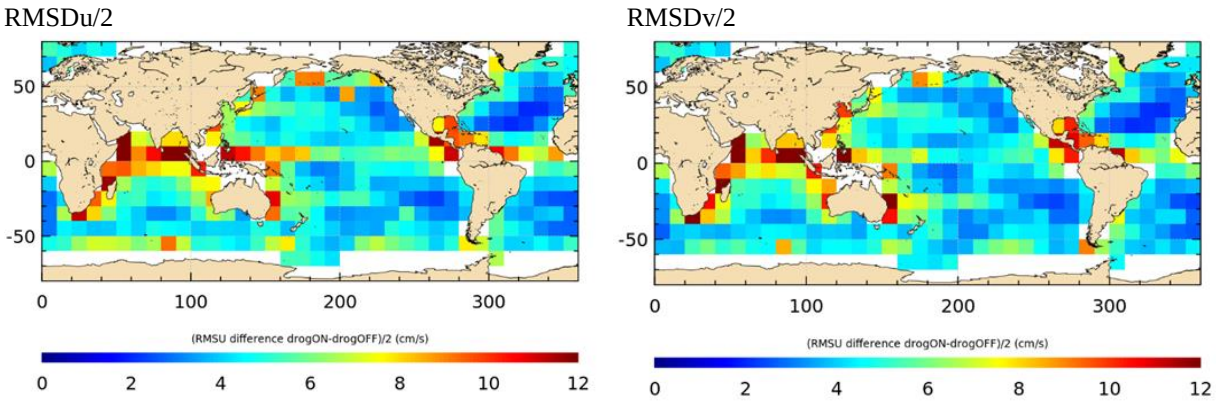

Figure 3-1: Error of mean current from drifters for (left) zonal and (right) meridional component (cm.s-1) in 10°x10° boxes where the number of observations is larger than 100

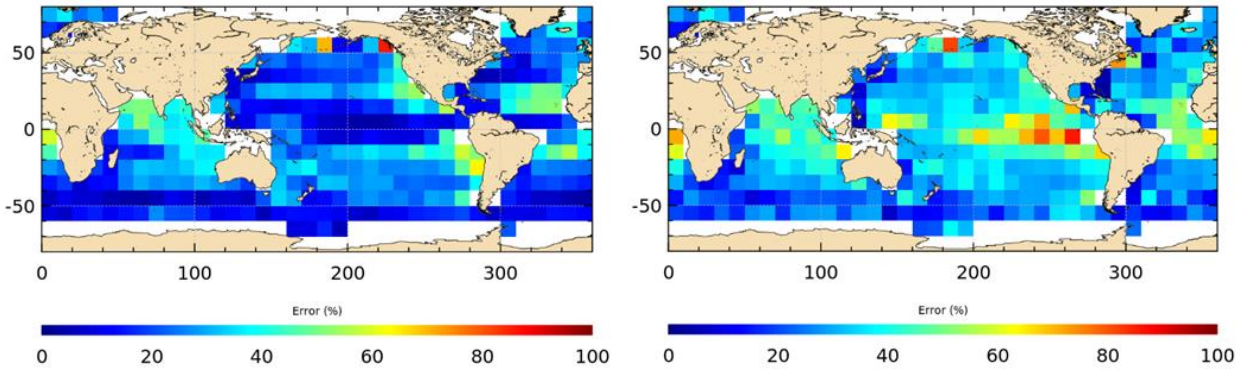

Figure 3-2: Error of mean current from drifters for (left) zonal and (right) meridional component in percentage of the signal (%) in 10°x10° boxes where the number of observations is larger than 100

3.2.3 Global Distribution and Statistics of the Reference Dataset

In the following we use "super observations" of mean geostrophic current estimated from both 15-m drogued and undrogued drifters starting at 400 km off the coast (Figure 3-3 and Figure 3-4). Indeed, filtering issues of MSS minus geoid height occur close to the coast. Moreover, as satellite-only geoid models are computed globally and indifferently for land and sea, we do not expect specific geoid model degradation in coastal area. Also, we do not consider the 5°S/5°N equatorial band since geostrophic assumption is no more accurate.

Figure 3-4 shows the number of super observations in 10°x10° boxes. Figure 3-5 shows the Root Mean Square of the mean geostrophic current estimated by the AOML drifters. The RMS is high in area of high spatial variability such as western boundary current, Antarctic Circumpolar Current (ACC) and Equatorial band for the zonal component. On the contrary the RMS is low at the interior of the gyre, especially in the Pacific for the meridional component.

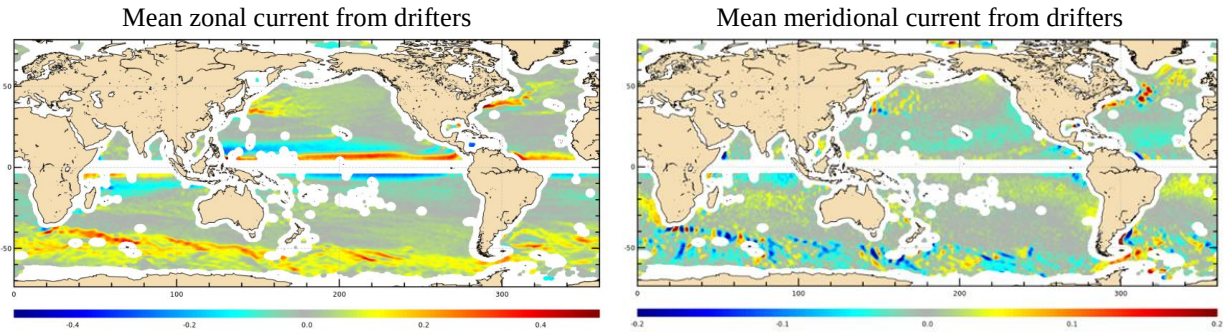

Figure 3-3: Mean geostrophic current filtered at 160km of wavelength and computed from 15m drogued and undrogued drifters at 400 km offshore the coast and out of the 5°S/5°N equatorial band (cm/s). Note that the range of the colour bar is ± 0.5 for the zonal component and ± 0.2 for the meridional component

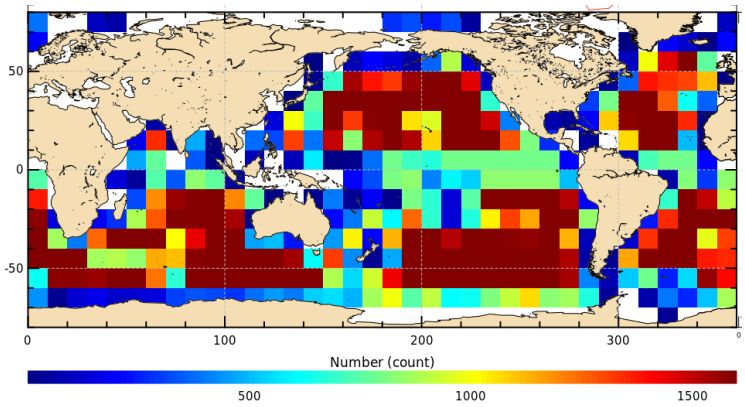

Figure 3-4: Number of "super observations" per 10°x10° boxes

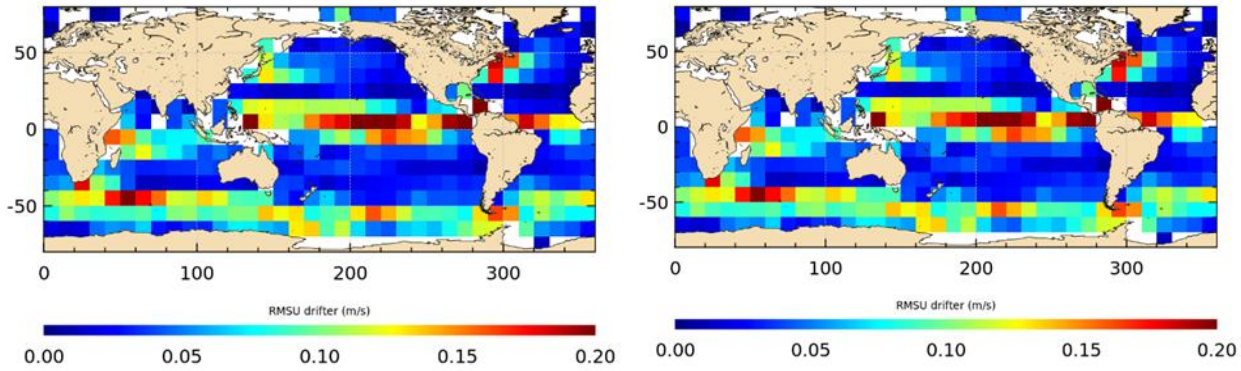

Figure 3-5: RMS of the mean geostrophic current estimated by the AOML drifters and computed in 10°x10° boxes for the (right) zonal and (right) meridional component

3.3 RESULTS

3.3.1 Global Statistics

In this part we compare mean geostrophic currents estimated from the geodetic MDTs filtered at different wavelength (160 km to 400km) with mean geostrophic currents estimated from drifters. The currents estimated from drifters can be either filtered at the same resolution as the geodetic MDTs or not.

Comparison with drifters filtered at the same scales than geodetic MDTs

Figure 3-6 and Figure 3-7 show the quadratic mean of the difference between mean geostrophic currents estimated from geodetic MDTs and the ones estimated from drifters both filtered at different wavelengths (160 to 400 km).

Figure 3-6 illustrates that GOCE data are able to resolve scales smaller than GRACE. At wavelength of 400km, performances of GRACE and GOCE are similar but at smaller wavelength MDT estimated using GOCE geoid model have smaller differences with drifters. Figure 3-6 illustrates also the improvement of the different GOCE releases especially

regarding the meridional currents. The quadratic means of the difference become smaller than 100% of the signal at the GOCE targeted wavelength of 200km with release 6.

Figure 3-7 focusses on the last releases 5 and 6. For zonal velocities performances are similar but for the meridional velocities improvement is significant with a quadratic mean of the difference that decrease from 90-100% to 60% at wavelength of 200km. Figure 3-7 shows also that between 250 and 400 km the quadratic mean is smaller with GOCE geoid model than with the state of the art combined geoid model EGM2008 that do not include GOCE data. Thus, even when the smaller scale of the geoid is contributed by altimetry, as in EGM2008, GOCE data are very valuable.

The quadratic means of the difference include different sources of error:

- Geoid commissioning error, but also
- MSS error,
- Filtering error (we use a Gaussian filter, which is not an ideal one),
- Error in the reference field: mean geostrophic current estimated from drifters (see section 3.2.2).

Thus the error of the mean geostrophic current computed from the last ESA HPF GOCE geoid model is less than 11% (60%) for the zonal (meridional) component at 200 km while it is less than 6% (22%) at 250 km. Note that velocities (gradient of the heights) are much more sensitive than height.

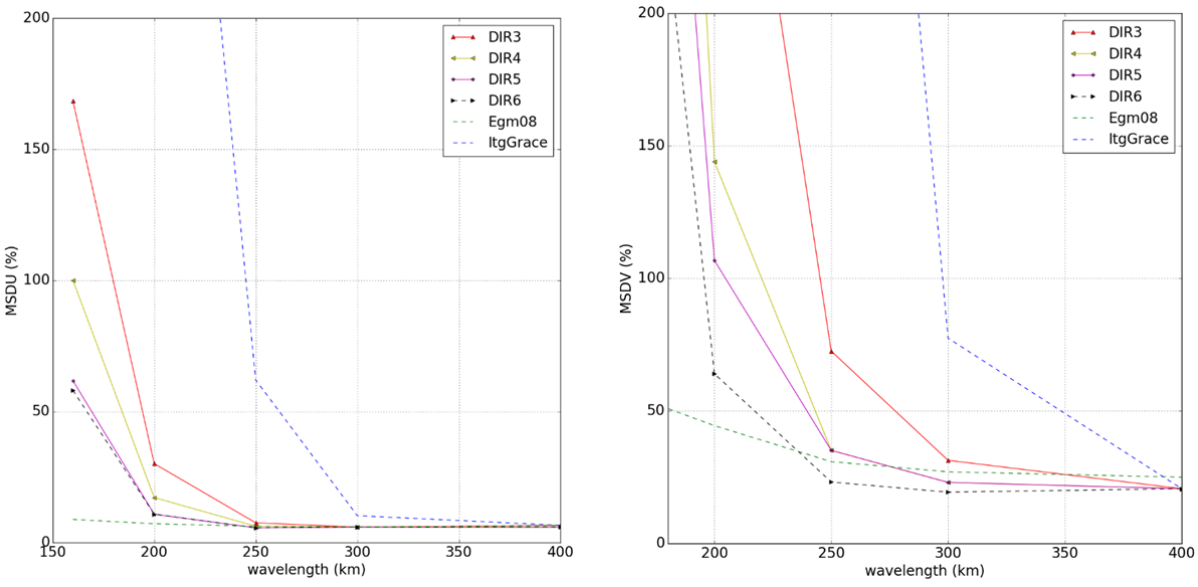

Figure 3-6: Quadratic mean of the difference between mean geostrophic currents estimated from geodetic MDTs and the ones estimated from drifters both filtered at different wavelengths (160 to 400 km). Statistics are expressed in percentage of the quadratic mean of the mean geostrophic currents estimated from drifters

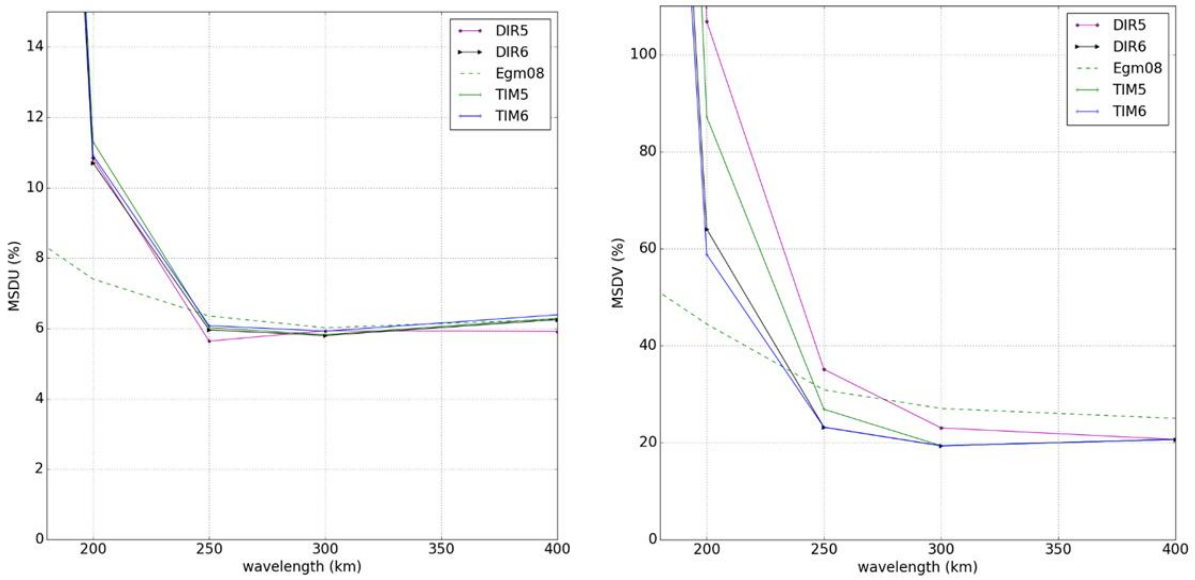

Figure 3-7: Same as Figure 3-6 but including geodetic MDTs from the Time-Wise solutions (TIM5 and TIM6)

Comparison with drifters filtered at 160km

In this part the comparisons are done with mean geostrophic current estimated from drifters and filtered at 160 km only. Thus, the quadratic mean of the difference include both, the commission and omission errors. As the commissioning error decreases with increasing wavelength (see previous section), the omission error increases. In this section we thus look for the optimal wavelength that minimizes both errors. Figure 3-8 shows that the quadratic mean is at a minimum at 250 km wavelength. In the following we will focus on this wavelength.

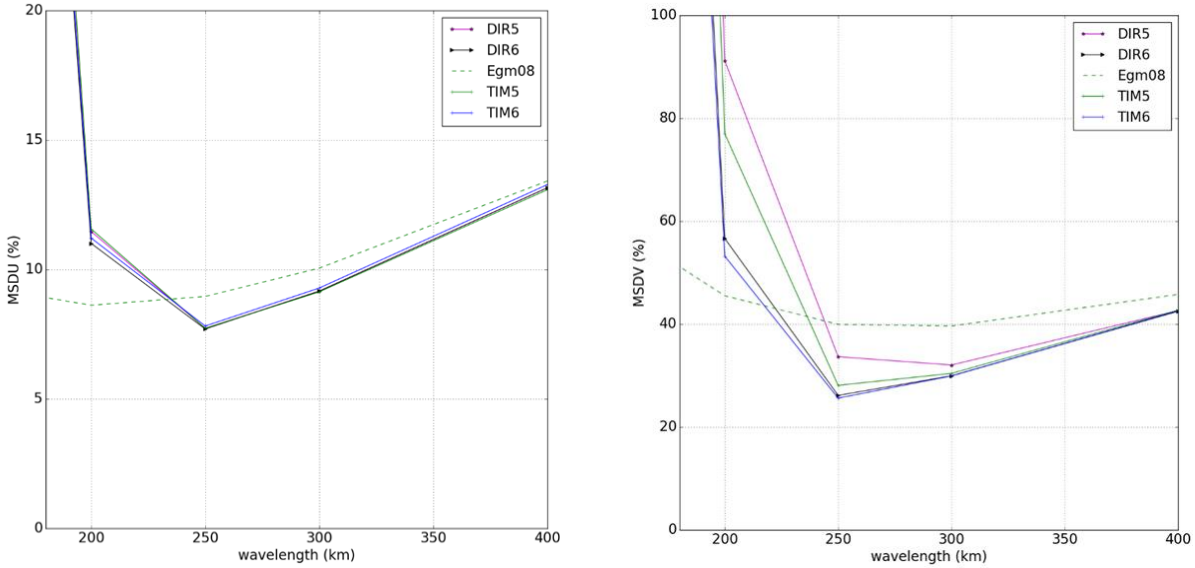

Figure 3-8: Quadratic mean of the difference between mean geostrophic currents estimated from geodetic MDT filtered at different wavelengths (160 to 400 km) and the ones estimated from drifters filtered at 160km. Statistics are expressed in percentage of the quadratic mean of the mean geostrophic currents estimated from drifters.

3.3.2 Statistics per 10°x10° Boxes at 250km of Wavelength

In this section we look at regional statistics (per 10°x10° boxes) at 250km wavelength. Figure 3-9 shows the quadratic mean of the difference of drifters to the geodetic MDT based on DIR6 and expressed in percentage while Figure 3-10 shows the Root Mean Square of the difference (RMSD) in m/s. Very similar results are found for TIM6. The results for the zonal component are quite spatially uniform compared with meridional component. For the zonal component, the quadratic mean is almost everywhere less than 50% and even less than 20% in most of the boxes. There are very few marginal boxes with a quadratic mean difference higher than 80% ; these boxes correspond to areas where the signal is low (i.e. low RMS in Figure 3-5) and moreover some are close to the equator (between 10°S and 5°S) where the geostrophic assumption vanishes. For the meridional component, there are more boxes with high quadratic mean of the difference. This is due to mainly two raisons. First, meridional velocities are less energetic (see Figure 3-5) and thus the ratio of noise versus signal is higher. Second, in the tropics this is due to residual noise as illustrated in Figure 3-11. Note however that compared with previous release 5, this last point has been improved. Indeed the difference of RMSE between the release 6 and 5 (Figure 3-12 and Figure 3-13) is negative in the tropics for the meridional component. The improvement is particularly significant for the direct method (DIR5 versus DIR6) since DIR5 was very polluted by vertical stripes (Figure 3-11and Figure 3-14).

Regarding the zonal component: there is no significant improvement of DIR6 compared with DIR5 (Figure 3-12). TIM is improved in the tropics and degraded at higher latitudes but the differences of RMSE are very small: between -0.25 and 0.25 cm/s except in some boxes close to the equator where the geostrophic assumption is less accurate (Figure 3-13). These are probably due to large scale difference between TIM5 and TIM6 (Figure 3-15) with lower geoid height within the tropics and higher geoid height at higher latitudes. This pattern is also seen when we compare TIM6 and DIR6 (Figure 3-16), while it was not seen in the previous release 5 models (Figure 3-17). Again, the differences are very small, ranging from -0.25 to 0.25 cm/s.

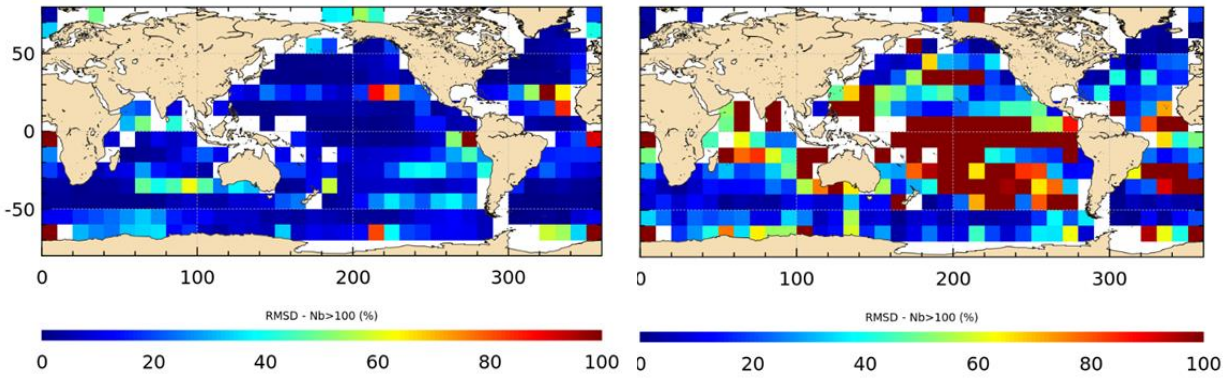

Figure 3-9: Quadratic mean of the difference between mean geostrophic currents estimated from geodetic DIR6 MDT and the ones estimated from drifters both filtered at 250km. Statistics are expressed in percentage of the quadratic mean of the mean geostrophic currents estimated from drifters. Only boxes where statistics are computed with more than 100 points are plotted

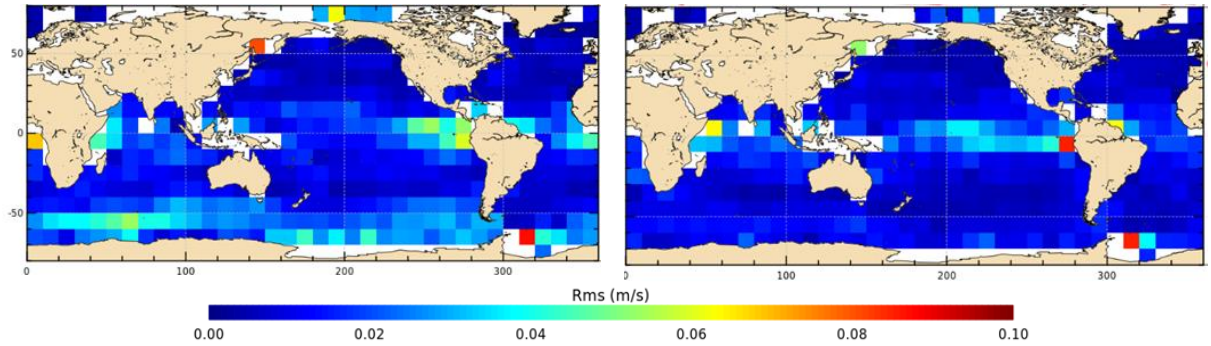

Figure 3-10: Root mean square of the difference between mean geostrophic currents estimated from geodetic DIR6 MDT and the ones estimated from drifters both filtered at 250km (m/s). Only boxes where statistics are computed with more than 100 points are plotted.

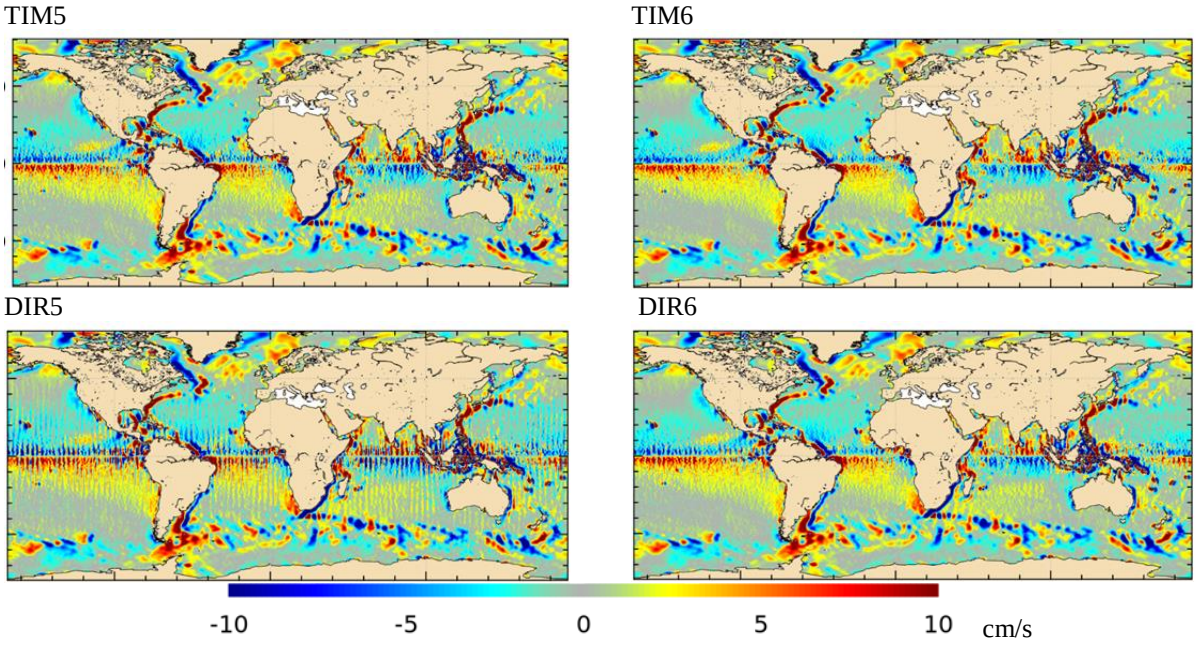

Figure 3-11: Meridional component of the mean geostrophic current associated with MDTs TIM5, TIM6, DIR5 and DIR6 filtered at 250km of wavelength (cm/s)

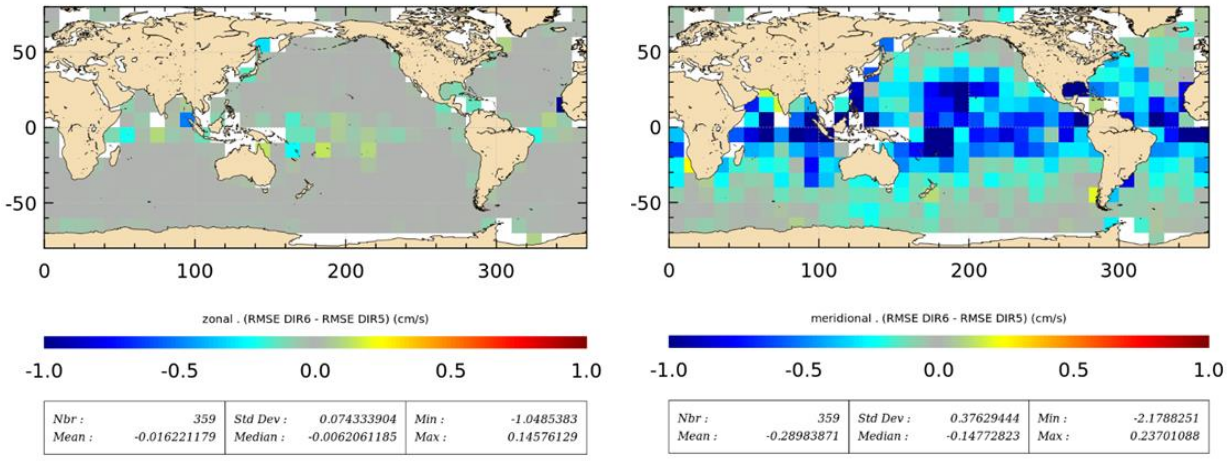

Figure 3-12: Difference of RMSE DIR6-DIR5 (cm/s)

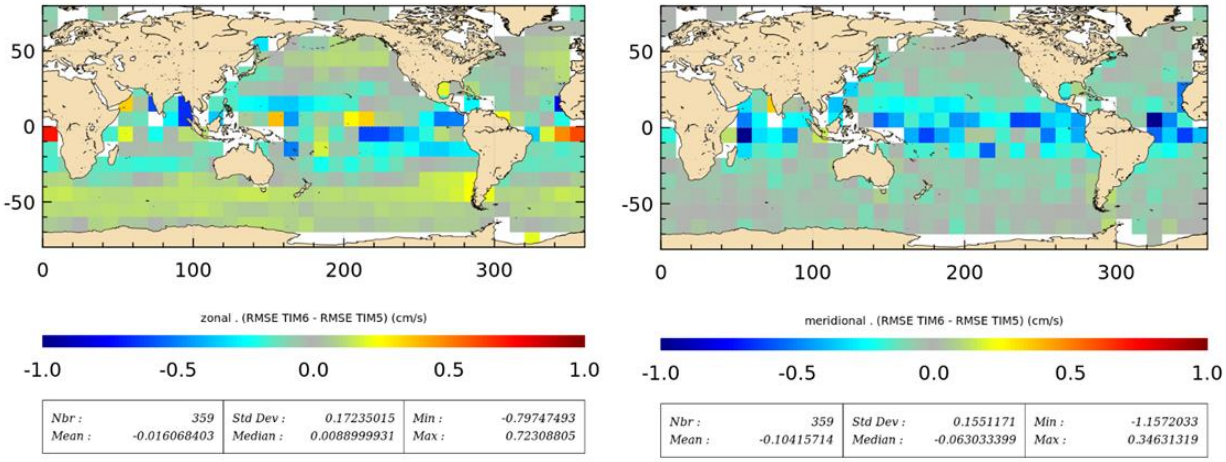

Figure 3-13: Difference of RMSE TIM6-TIM5 (cm/s)

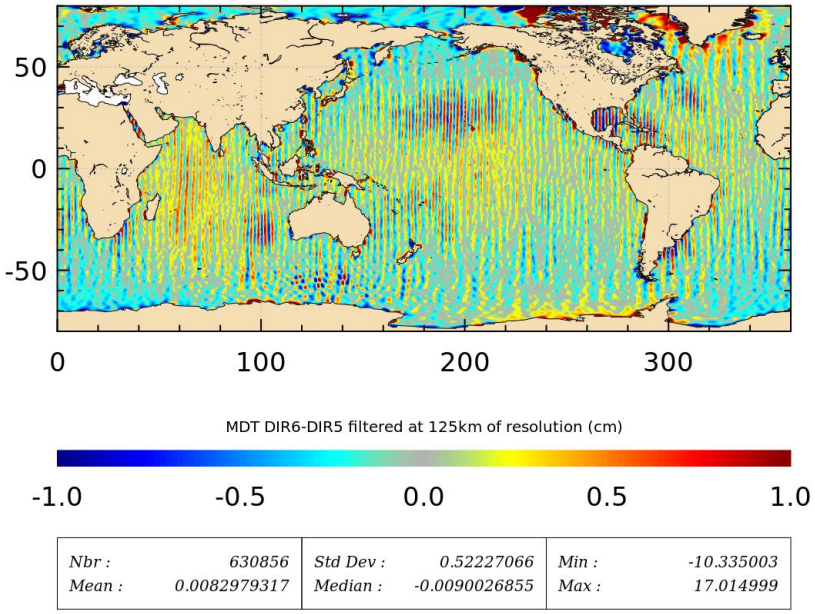

Figure 3-14: Difference between the geodetic MDT from DIR6 and the one from DIR5 at wavelength 250 km

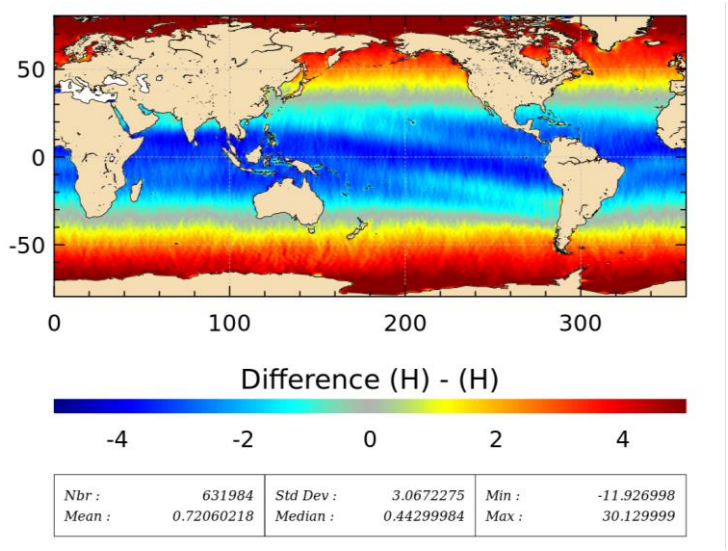

Figure 3-15: Difference between the geodetic MDT from TIM6 and the one from TIM5 at 250 km wavelength

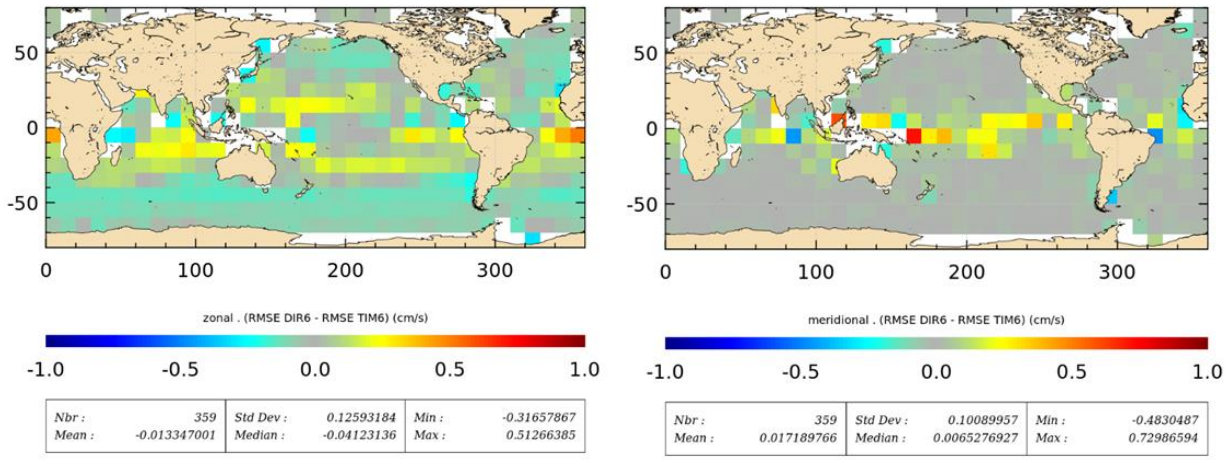

Figure 3-16: Difference of RMSE DIR6-TIM6 (cm/s)

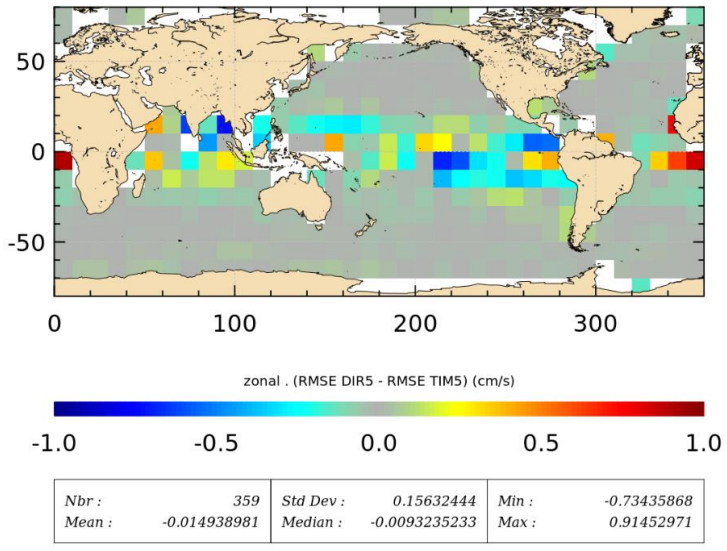

Figure 3-17: Difference of RMSE DIR5-TIM5 (cm/s)

3.3.3 Statistics per 10°x10° Boxes at 160km and 200km of Wavelength

Section 3.3.1 showed that the optimal wavelength of MDTs based on GOCE geoid models is 250km globally. The previous section showed that even at 250km wavelength the meridional component of the velocities is not well resolved in the Tropical South Pacific since the signal is very small. On the contrary, this section 3.3.3 investigates if in some areas MDTs using GOCE data are able to resolve signal at wavelength smaller than 250km.

Figure 3-18 and Figure 3-19 show the quadratic mean of the difference of geostrophic currents between MDT computed from DIR6 and the drifters, both filtered respectively at 160 and 200 km wavelength. At 160km: only some part of the very energetic currents (Antarctic Circumpolar Current and western boundary currents) are in agreement with the drifters for both zonal and meridional component (the quadratic mean of the difference is smaller than 100%). At 200km, these very energetic currents are well resolved with a quadratic mean of the differences smaller than 60% in most boxes covered by these currents. Regarding the zonal component, at 200km most of the boxes show a quadratic mean of the difference smaller than 60% except in the interior and East of the gyres.

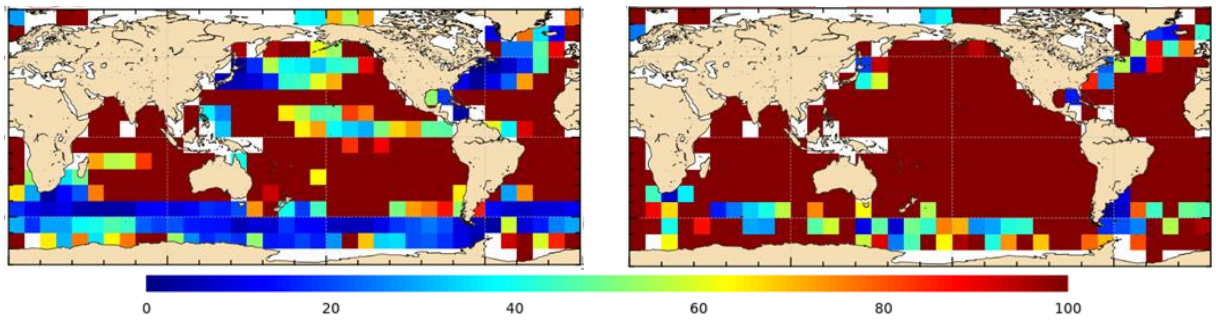

Figure 3-18: Quadratic mean of the difference between mean geostrophic currents estimated from geodetic DIR6 MDT and the ones estimated from drifters both filtered at 160km of wavelength. Statistics are expressed in percentage of the quadratic mean of the mean geostrophic currents estimated from drifters

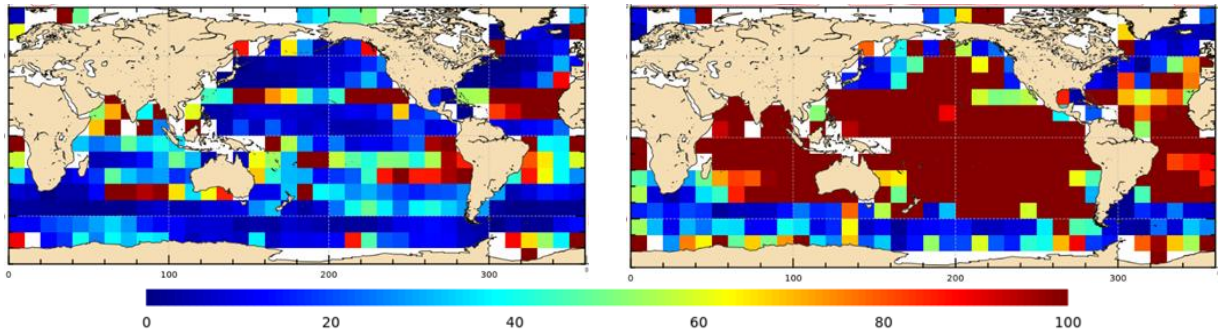

Figure 3-19: Quadratic mean of the difference between mean geostrophic currents estimated from geodetic DIR6 MDT and the ones estimated from drifters both filtered at 200km of wavelength. Statistics are expressed in percentage of the quadratic mean of the mean geostrophic currents estimated from drifters.

3.4 CONCLUSIONS

In thus study we tested geoid models DIR3, DIR4, DIR5, DIR6, TIM5, TIM6, ITG-Grace and EGM2008 to compute geodetic MDTs and associated mean geostrophic currents. These currents were then compared with independent estimates from AOML/SVP drifters.

As expected, the MDTs that use GOCE data resolve smaller scales than when using only GRACE data: at wavelengths smaller than 400km, MDTs estimated using GOCE geoid model have smaller differences with drifters.

Comparison with the reference model EGM2008 shows that it is important to use GOCE between 250 and 400 km wavelengths, even in a combined geoid model.

Then, the comparison with drifters illustrates the improvement of the different ESA HPF GOCE releases. Globally, the minimum quadratic mean of the difference with drifters filtered at wavelength 160km is reached for MDTs filtered at 250km. For this optimal wavelength, mean geostrophic currents estimated from GOCE6 reach a ratio noise over signal smaller than 8% (25%) for the zonal (meridional) component.

However, this 250km optimal wavelength is estimated using a Gaussian filter that is not ideal. Also, the performances depend on the area: there is residual noise mainly in the tropics for the meridional component whereas in more energetic areas such as the Circumpolar or western boundary currents performances are good at 200km and even at 160km for the zonal component. Thus, when using GOCE to estimate oceanic circulation we recommend using an adaptative filter regarding the area. For instance, Knudsen et al. (2019) adapt the scale of the filter using comparison with drifters while Rio et al. (2014, 2019) use comparison with other MDTs.

Note however that geoid gradients are much more sensitive to noise than the geoid height itself. Moreover, as we look at geostrophic velocities, the gradient of the height is multiplied by g/f (see equation (1)), with f decreasing toward 0 at the equator. Thus, the differences with drifters will be even greater as we look closer to the equator because they are weighted by the factor 1/f.

4. MODEL VALIDATION BY MEANS OF GNSS-LEVELLING

4.1 METHOD

The absolute accuracy is assessed by comparison of model derived geoid heights (or height anomalies) to independent geoid heights at GNSS-levelling stations. The procedure follows to a large extent the method as described in Gruber and Willberg (2019) and in Gruber et al (2011). As it is quite important to interpret these differences in a correct way the basic processing steps are described here again.

Step 1: Spherical harmonic coefficients need to be transformed to the constants of the reference ellipsoid of the GNSS observations. Normal gravity field and geometric reference ellipsoid (semi major axis) need to be consistent. In addition, the spherical harmonic series needs to be transformed to the permanent tide system of the GNSS levelling points (if required) (Gruber et al, 2014).

Step 2: Computation of geocentric coordinates for the GNSS-levelling points from ellipsoidal coordinates observed by GNSS and solution of the spherical harmonic series of the gravity field model at this location on the Earth surface up to degree N for height anomalies (Gruber et al, 2014).

Step 3: Estimation of the omission error, i.e. the gravity field signal not represented by the spherical harmonic series as it is used in step 2 (up to degree N). The main component is computed from an existing high resolution gravity field model up to degree 2190. In case N is below the maximum degree of this high resolution model, the omission error is computed from degree N+1 to the full resolution of the model (e.g. degree 2190). In addition, the remaining omission error above the maximum degree is computed from a topographic gravity field model estimating the gravity signal from the residual topography above the maximum resolution of the high resolution gravity field model. Here we use the ERTM2160 model (Hirt et al, 2014). This model represents the short scale Earth gravity field above degree and order 2160 computed by forward modelling of an improved Shuttle Radar Topography Mission (SRTM) topography model and spectral filtering. It shall be noted that the spectral content of the high resolution gravity field models is limited to degree and order 2160. The coefficients between degree 2160 and 2190 are artificially generated from the conversion of ellipsoidal harmonics into the spherical domain.

Step 4: In case orthometric height at GNSS-levelling points are available an additional correction needs to be applied to the height anomalies computed from the global model in order to get geoid heights. This term, also called geoid-quasi geoid separation, is computed according to Rapp et al (1997) and is strongly dependent on the height of the GNSS-levelling point. As the density of the topography and its variations between the Earth surface and the geoid is not known, the geoid-quasi geoid separation term degrade the quality of the reference geoid heights in mountainous areas. This needs to be considered when the differences between observed, and from global models computed, geoid heights are analysed.

Step 5: These height anomalies or geoid heights then can be directly compared to the corresponding results at the GNSS-levelling points, which are computed by subtracting the orthometric height or the normal height from the ellipsoidal GNSS height. These differences

can be analysed per regional data set either by regarding the difference maps or by statistical analyses.

Step 6: In many cases the differences for a regional data set exhibit systematics in terms of biases or tilts. Biases are caused by different definitions of national height systems, but can be neglected for the validation of global gravity field models as long as the bias for a regional data set is constant. Tilts, on the other hand, can be caused by a deviation of the national height reference surface from an equipotential surface or by systematic errors in the spirit levelling network (Wang et al, 2012). For validation of global gravity field models these effects need to be accounted for by disregarding the mean difference (i.e. the bias) and by computing a planar correction surface which is applied to the height anomalies or geoid heights, respectively.

Step 7: After applying the correction surface the root mean square (RMS) of the differences between the model geoid and the observed GNSS-levelling geoid is computed per region as a validation result. The RMS value is a quality criterion which tells how good the global model fits to the observed geoid or height anomalies.

The procedure as described above is applied to a number of available GNSS-levelling data sets, which are introduced in the following chapter.

4.2 GNSS-LEVELLING DATA

Table 4-1: Overview of GNSS-Levelling datasets used for the comparisons

Region	No. Points	Reference
Australia	197	Geoscience Australia, 2003
Brazil	683	Brazilian Institute of Geography and Statistics - IBGE, Directorate of Geosciences - DGC, Coordination of Geodesy – CGED, 2012
Canada	579 2576	National Resources of Canada (NRCan), via US NGS, 2012 National Resources of Canada (NRCan), 2007
Europe various countries, EUREF EUVN	1233	Bundesamt für Kartographie und Geodäsie, Frankfurt/Main, 2007
Germany	675 470	Bundesamt für Kartographie und Geodäsie, Frankfurt/Main, 2003 © GeoBasis-DE / Geobasis NRW, 2018
Great Britain	177	UK Ordnance Survey, 2011
Greece (mainland)	1542	Aristotle University of Thessaloniki, 2016
Japan	837	Japanese Geographical Survey Institute, 2003
Mexico	744	Instituto Nacional de Estadística y Geografía (México) via US NGS, 2012
Saudi Arabia	382	King Abdulaziz City for Science and Technology KACST, 2012
USA	24872	National Geodetic Survey (NGS), 2012

Various sets of GNSS-levelling data are used, which are summarized in Table 4-1. In general, these data sets are provided in the form of orthometric heights from the spirit levelling, which are subtracted from the ellipsoidal heights from GNSS in order to compute geoid heights. Only for Germany and the unified European data set normal heights and height anomalies are available. The number of stations and subsequently their density in each region vary significantly (refer to Table 4-1, column 2).

4.3 RESULTS

The quality of the high resolution gravity field models is assessed by comparisons to independently observed geoid heights at GNSS-levelling stations. The procedure is described in detail in chapter 4.1, while the GNSS-levelling data sets are summarized in Table 4-1. First, for two regional examples, the raw differences are computed, the estimated planar correction surface is estimated and residual differences after applying the correction surfaces are computed.

Here we use the US data set from 2012 and the German data set from 2018 (refer to Table 4-1) as well as a high resolution gravity field model which was computed in the frame of the ESA project and named GOCE-OGMOC (refer to Gruber and Willberg, 2019). This model is a combination between the XGM2016 (Pail et al, 2018) and the EIGEN6-C4 model (Förste et al, 2014). It is identical to XGM2016 up to degree 619, between degree 620 and 719 both models are spectrally combined applying a weighting function and from degree 720 to 2190 it is identical to EIGEN6-C4. Both models include identical altimetric gravity anomalies, while over land an improved 15'x15' block-mean data set of gravity anomalies provided by the National Geospatial-Intelligence Agency (NGA) was used for XGM2016. This data set was extracted from the NGA database of terrestrial and altimetric gravity data and incorporates in some regions newly observed gravity data from airborne campaigns. In addition, improved data editing and preparation were applied to the data before the calculation of the block-mean values. In the spectral range from degree 620 to 2190, according to the weights, terrestrial information (over land) from the EGM2008 model is introduced over land. As satellite information a GRACE/GOCE combination model was used, which includes the complete GOCE mission data set and most of the GRACE data (GOCO05S, Mayer-Gürr et al, 2015).

4.3.1 Correction Surface

Figure 4-1 and Figure 4-2 show the results of the pointwise geoid differences between the DIR6 model up to degree 200 (taking into account the remaining omission error from the GOCE-OGMOC and the residual topographic gravity model) and the independent geoid heights observed at the GNSS-Levelling stations before and after applying the planar correction surface and the correction per point. It is obvious that for the US data set there are large systematic differences between both data sets (see Figure 4-1 middle row), which cannot origin from the global model, but must be caused by the GNSS-Levelling derived geoid heights. As these are computed from GNSS ellipsoidal heights and levelled orthometric heights such large differences only can be caused by levelling errors or errors related to the definition of the height system (e.g. bias). GNSS observations do not exhibit such systematic problems. In the case of the German data set the systematic differences are much smaller, but still visible in the range of a 6 cm tilt from North to South (Figure 4-2 top right). So even for this high quality data set there exist remaining systematic differences. For the reason that it

can be assumed that they are caused by the levelling and not by the global models, the planar correction surface is subtracted from the raw geoid differences in order to eliminate such problems. The residual differences as shown in Figure 4-1 and Figure 4-2 show geoid differences which can be addressed to errors of the global models, of the GNSS observations, of remaining random errors of the levelling and to errors of the models used for estimating the omitted signal. The range of the absolute differences now is at a level of ±20 cm for the US data set and ±5 cm for the German data set. Specifically the latter already shows very good performance of the GOCE model.

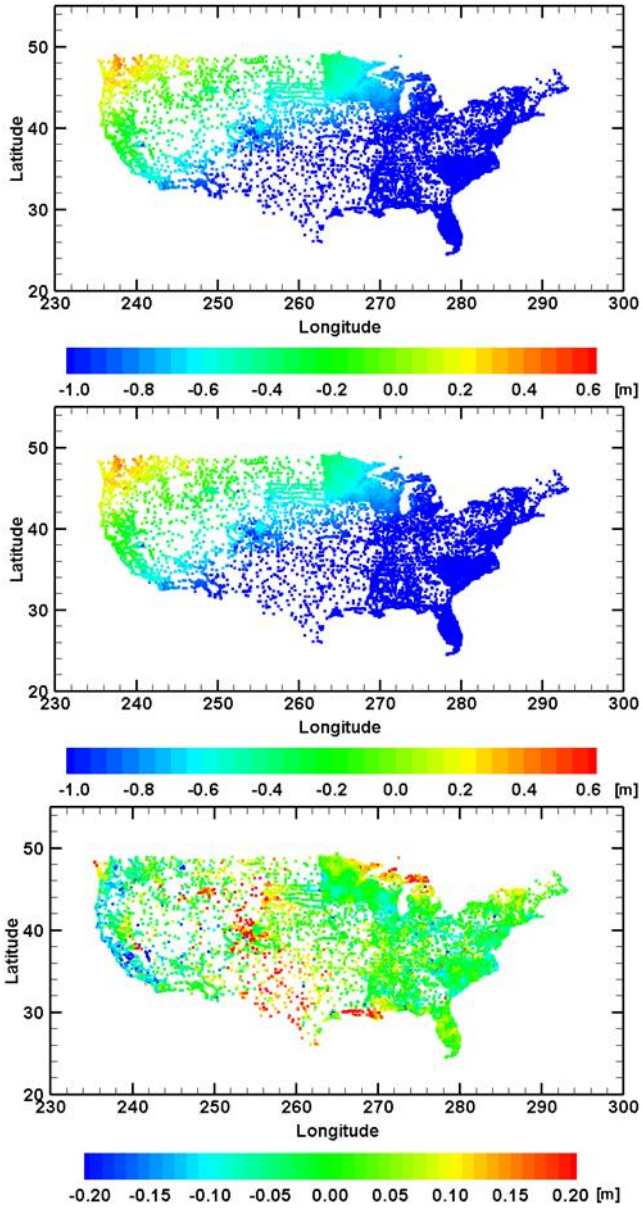

Figure 4-1: Differences of GOCE DIR6 model to USA 2012 GNSS-Levelling data. The DIR6 model was used up to degree and order 200. Omission error is estimated from the GOCE-OGMOC high resolution model. Top: Raw differences without applying planar correction surface; Middle: Correction surface at GNSS-levelling points; Bottom: Residual differences after applying the correction surface.

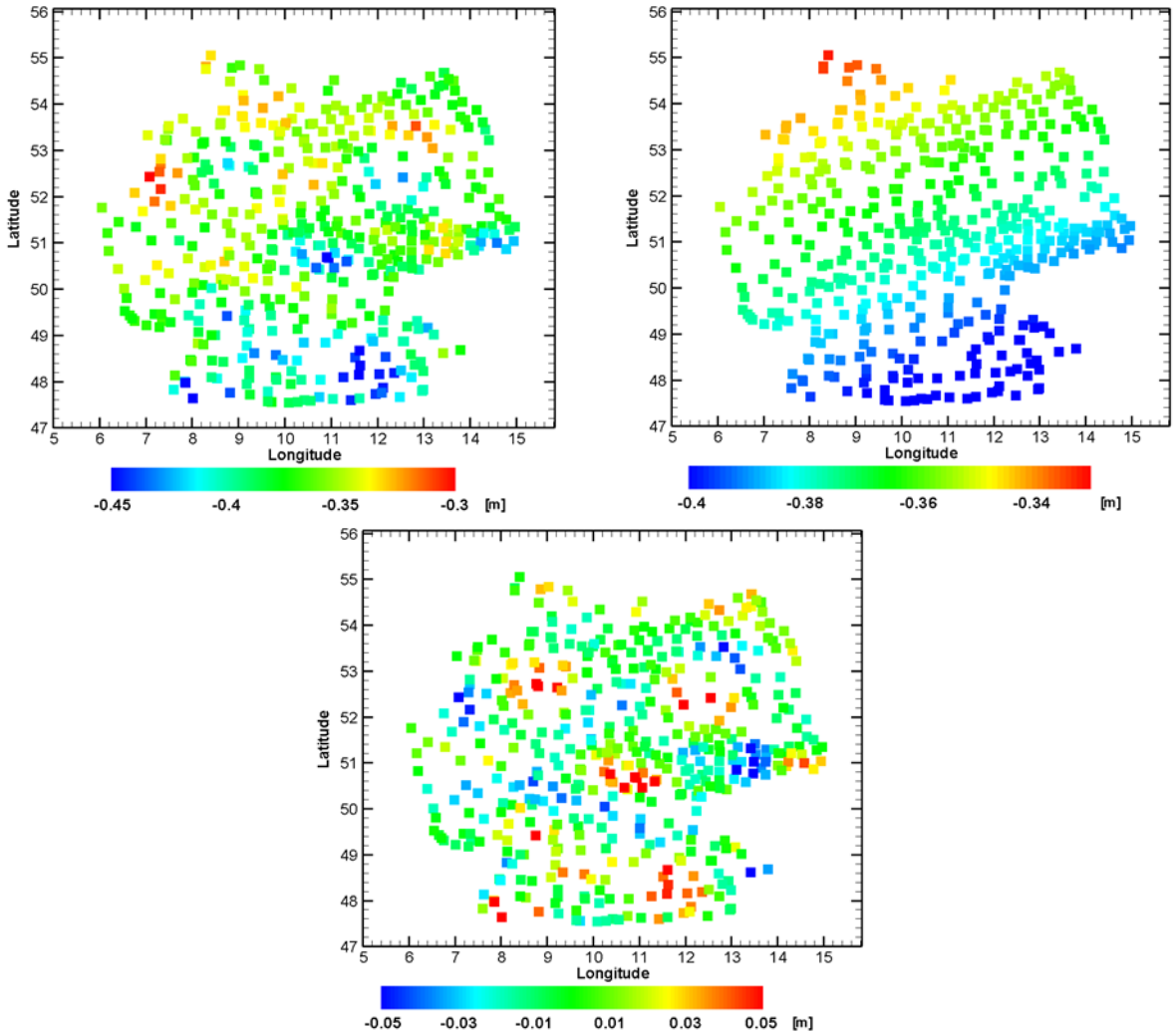

Figure 4-2: Differences of GOCE DIR6 model to German 2018 GNSS-Levelling data. The DIR6 model was used up to degree and order 200. Omission error is estimated from the GOCE-OGMOC high resolution model. Top left: Raw differences without applying planar correction surface; Top right: Correction surface at GNSS-levelling points; Bottom: Residual differences after applying the correction surface.

4.3.2 Differences Models to GNSS-Levelling Geoid

The global models performance is evaluated by differences to GNSS-Levelling observed geoid heights for different truncation degrees. The omission error above the truncation degree is computed from a high resolution model (in this case the GOCE-OGMOC model is taken) and from the residual topographic gravity potential (refer to chapter 4.1). The impact of the truncation degree is investigated by applying different truncation degrees (degree 10 to 300 in steps of 10). For each region and for each truncation degree the RMS of geoid differences between the model and the GNSS-levelling data is computed (in all cases the planar correction surface was applied). The following figures show the RMS of these differences depending on the truncation degree for various regional GNSS-Levelling data sets.

Before drawing any conclusion from the results, Figure 4-3 and Figure 4-4 shall be explained shortly. In each sub-plot the red horizontal line represents the model used for computing the omission error. As the GOCE-OGMOC model (which is up to degree 620 identical to the XGM2016 model and therefore in the figures it is named XGM2016) was used the RMS of the GOCE-OGMOC truncated model enhanced by the GOCE-OGMOC omission error always represents the full model. Therefore, for GOCE-OGMOC (XGM2016) the RMS of the geoid differences is identical for all truncation degrees. Results can be interpreted by a relative comparison of the XGM2016 line with the results for the DIR and TIM models. In case a model line is below the red line this model for this degree of truncation fits better to the GNSS-levelling geoid heights and vice versa.

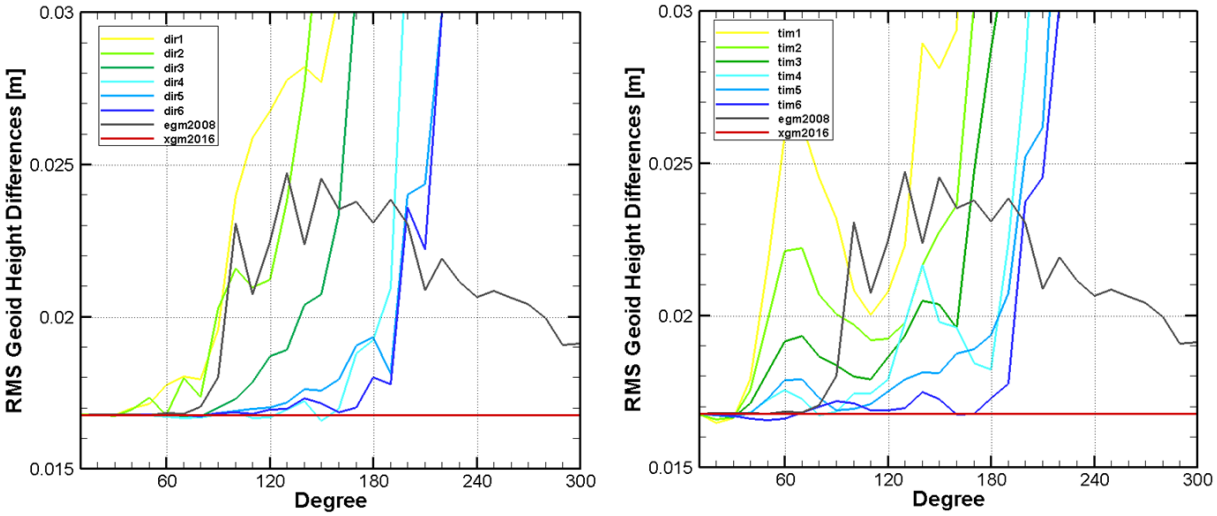

Figure 4-3: RMS of geoid height differences for German 2018 GNSS-Levelling data set for the DIR model series (left) and the TIM model series (right). As references the EGM2008 and the XGM2016 combined models are shown as well.

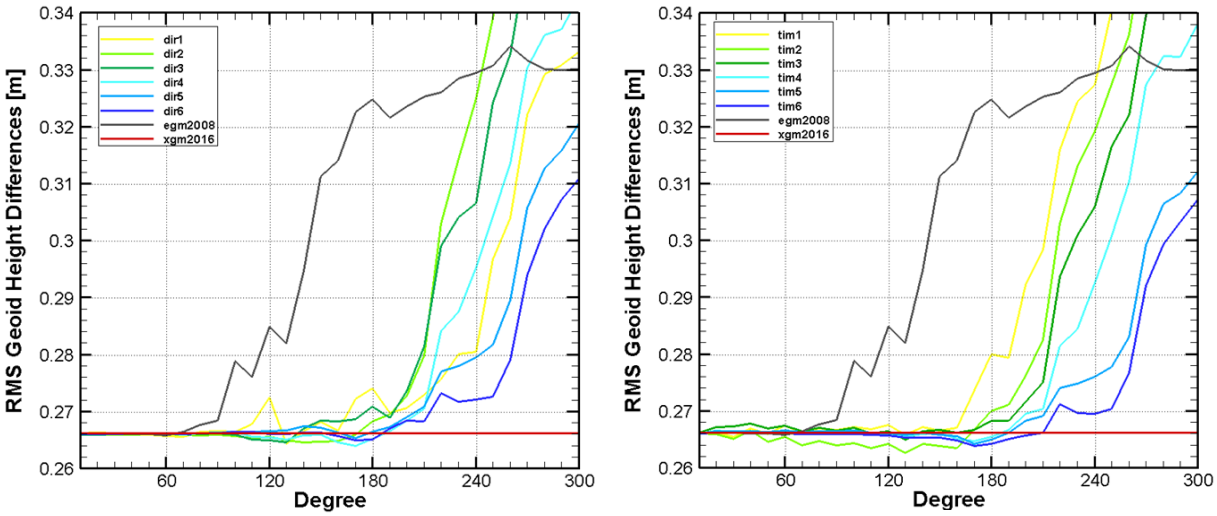

Figure 4-4: RMS of geoid height differences for Brazilian GNSS-Levelling data set for the DIR model series (left) and the TIM model series (right). As references the EGM2008 and the XGM2016 combined models are shown as well.

From a detailed analysis of the results shown in Figure 4-3 and Figure 4-4 the following conclusions can be drawn:

- One can observe that for all truncation degrees between 100 and 220, EGM2008 exhibits larger RMS values than all other models. This clearly indicates the impact of GOCE (and partially GRACE) satellite data, which were not used in EGM2008.
- For both model series it can be identified that with each new release the model fits better to the GNSS-Levelling geoid heights. This clearly shows the improvements by adding more data, but also due to the gradients reprocessing. Release 6 specifically outperforms the release 5 models even if they are based on the same amount of data. This improvement can be completely addressed to the improved gravity gradients from the reprocessing campaign.
- For the Brazilian data set the rel. 6 models improve by roughly 6 cm with respect to EGM2008 up to degree 220. But it can also be noticed that the average RMS value is relatively high (26.5 cm), which is caused by the poorer quality of the Brazilian levelling data if they are regarded over the whole country.
- The comparisons to the 2018 German GNSS-Levelling geoid heights, which are determined from a complete re-observation during the years 2014 to 2016, we can identify a very low average RMS (at a level of 1.7 cm). The rel. 6 GOCE models are close to the reference model (red line) up to degree 190. This means that up to this resolution the DIR6 and the TIM6 seem to have full signal content.

The following figures show the results only for the release 5 and release 6 models together with the two reference models. This enables a better comparison of the impact of the reprocessing campaign.

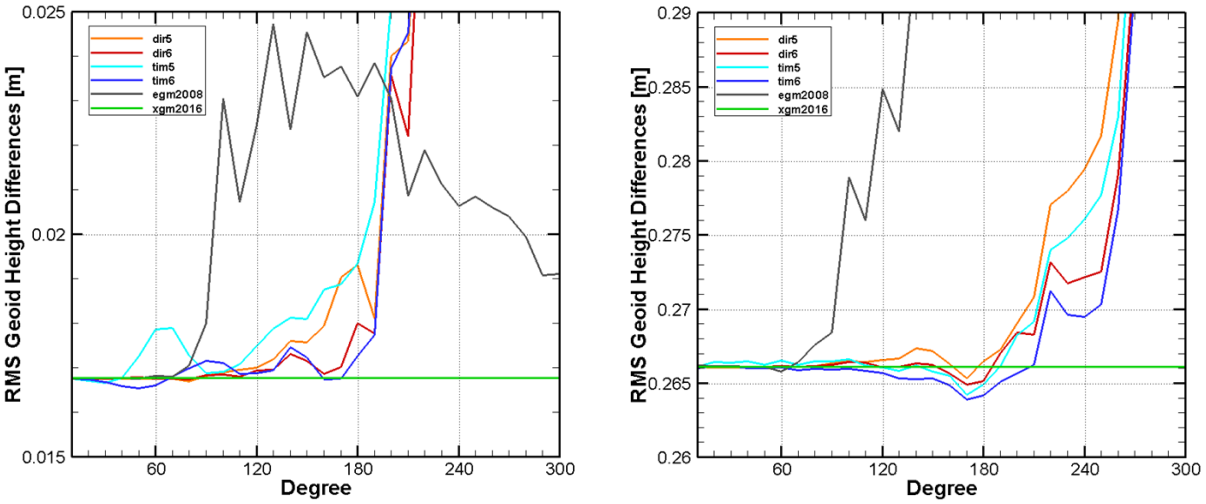

Figure 4-5: RMS of geoid height differences for the DIR5, DIR6, TIM5 and TIM6 models. **Left: Germany 2018**; **Right: Brazil**. As references the EGM2008 and the XGM2016 combined models are shown as well.

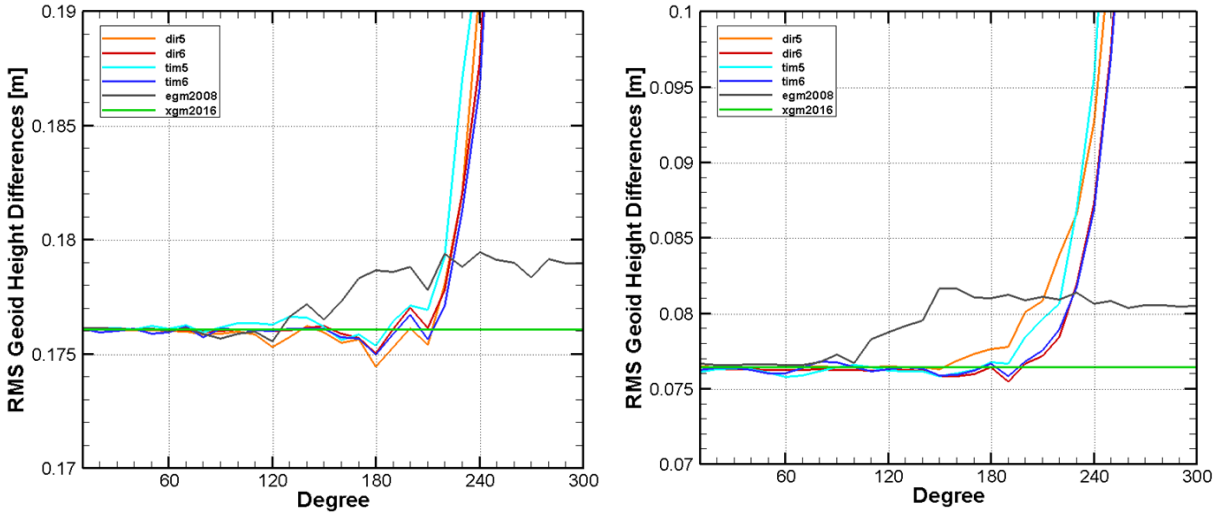

Figure 4-6: RMS of geoid height differences for the DIR5, DIR6, TIM5 and TIM6 models. **Left: Australia**; **Right: Canada 2012**. As references the EGM2008 and the XGM2016 combined models are shown as well.

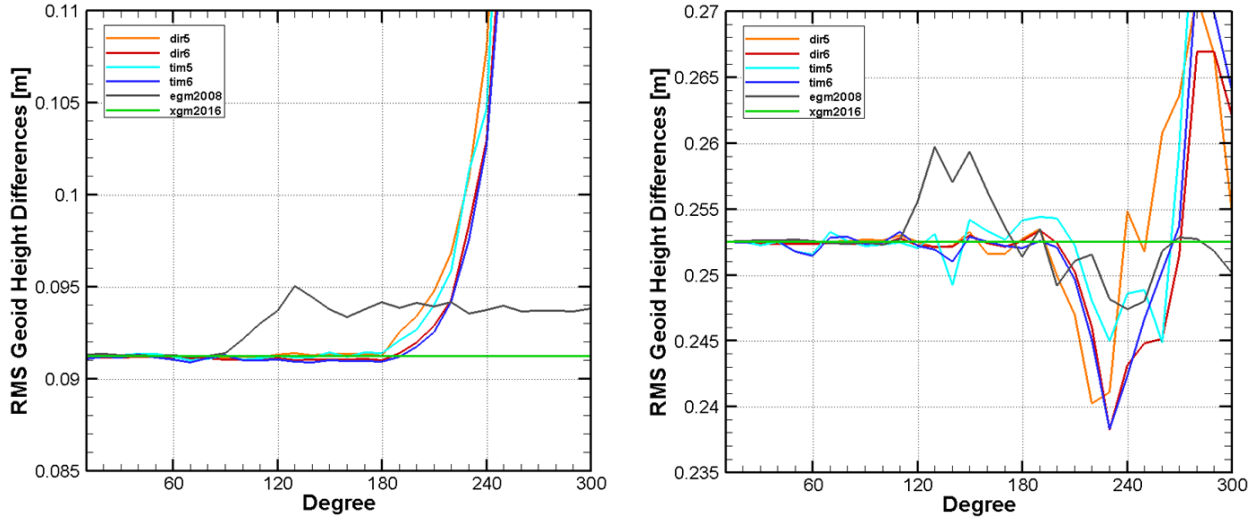

Figure 4-7: RMS of geoid height differences for the DIR5, DIR6, TIM5 and TIM6 models. **Left: Continental USA 2012**; **Right: Alaska 2012**. As references the EGM2008 and the XGM2016 combined models are shown as well.

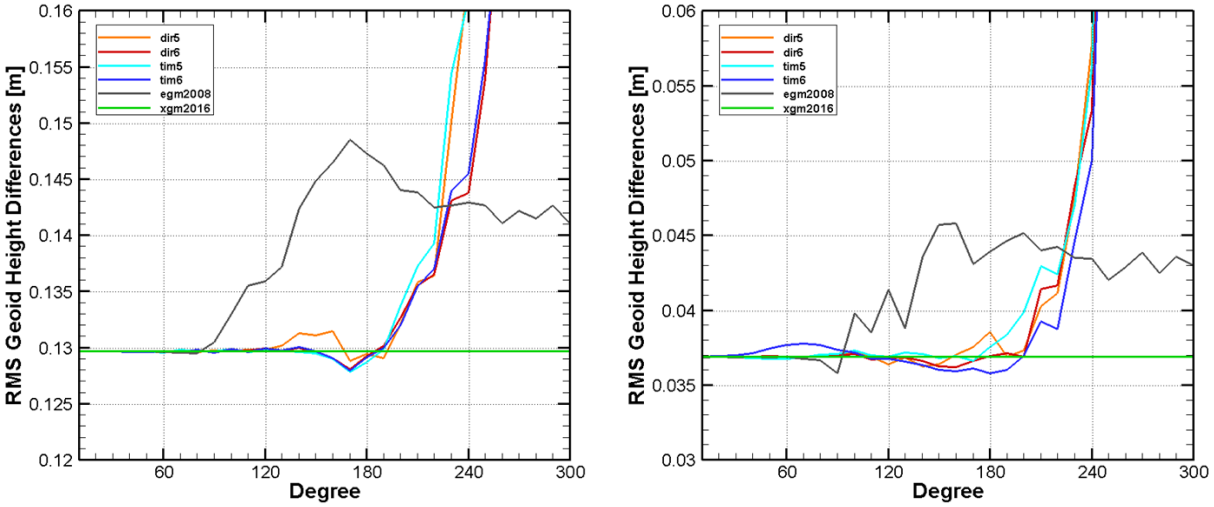

Figure 4-8: RMS of geoid height differences for the DIR5, DIR6, TIM5 and TIM6 models. **Left: Greece**; **Right: UK**. As references the EGM2008 and the XGM2016 combined models are shown as well.

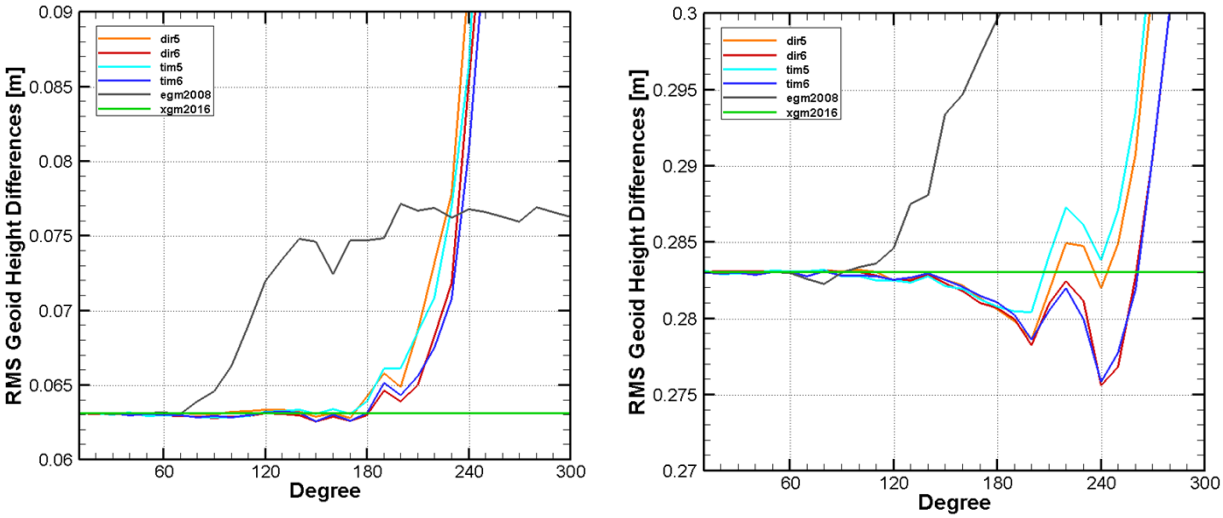

Figure 4-9: RMS of geoid height differences for the DIR5, DIR6, TIM5 and TIM6 models. **Left: Japan**; **Right: Mexico**. As references the EGM2008 and the XGM2016 combined models are shown as well.

From Figure 4-5 to Figure 4-9 the following conclusions can be drawn:

- The rel. 6 GOCE models show for all comparisons better (or sometimes equal) performance as the rel. 5 models. This specifically is visible at the higher truncation degrees indicating that the rel.6 models contain more signal than the rel. 5 models.
- In all cases the GOCE models are significantly better than the EGM2008 model, which is not based on GOCE data. This already is visible at medium truncation degrees (e.g. starting from degree 60). This clearly indicated the value of GOCE for the static field.
- In some areas the rel. 6 GOCE models even outperform the XGM2016 model despite that this model is based on a quasi complete GRACE data set, the complete GOCE original gravity gradients and up to date terrestrial data. For some data sets this is

clearly visible for higher truncation degrees, but in some cases even the lower truncation degrees are improved slightly.

- For the lower truncation degrees (e.g. up to degree 120) in some areas one can identify that the DIR6 model performs slightly better than the TIM6 model. Sometimes the TIM6 model exhibits some kind of small wave between degree 0 and 120. This is an indicator that for the longer wavelengths the combination with GRACE helps to estimate the lower degrees better than just from the GOCE data. This is well known as for the pure GOCE model (TIM6) the longer wavelengths are mostly determined from high-low satellite-to-satellite tracking data, while for the DIR6 model the complete reprocessed GRACE data set has been included.

4.3.3 Assessment of Absolute Accuracy

As it was identified in the previous sections one could state that the GNSS-Levelling data set in Germany obviously is the best available independent geoid data set. Therefore, this data set is used to estimate the absolute geoid error of the GOCE fields in this area and to identify if the estimated geoid errors are realistic. For this purpose the results shown in Figure 4-5 shall be investigated in more detail. Figure 4-10 is a copy of Figure 4-5 and includes now the numbers of the RMS values for the geoid differences at specific resolutions. Degree 190 corresponds to a spatial resolution of about 105 km at the equator and degree 200 to 100 km, respectively.

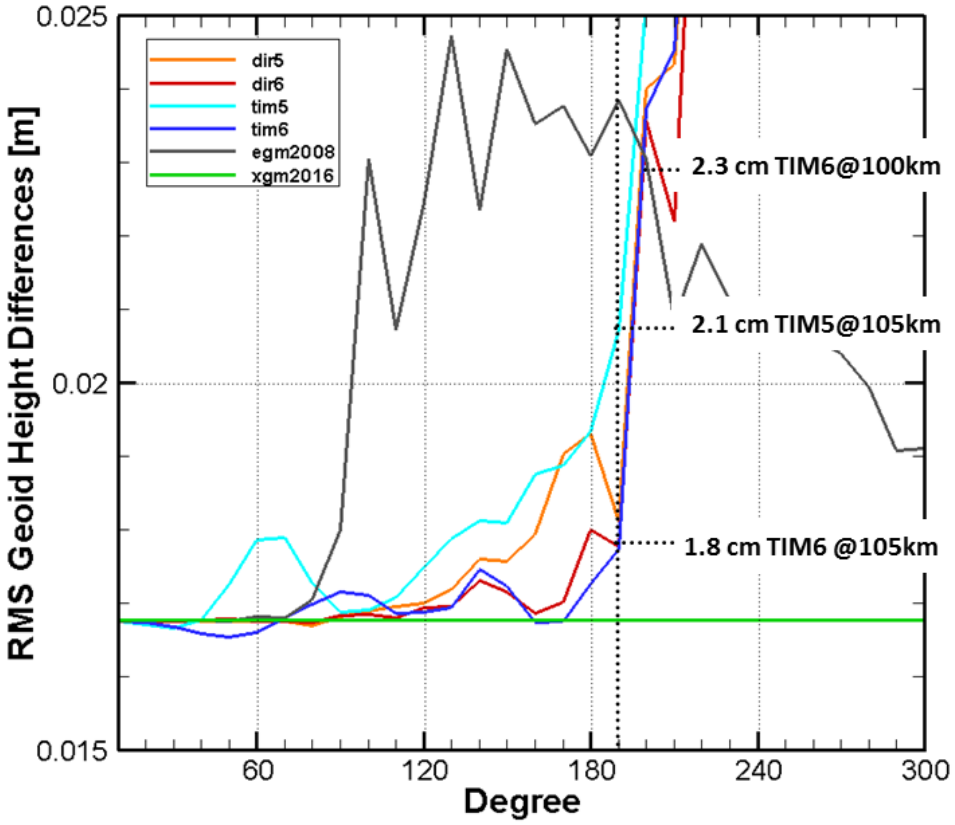

Figure 4-10: RMS of geoid height differences for the DIR5, DIR6, TIM5 and TIM6 models for the German 2018 data set. As references the EGM2008 and the XGM2016 combined models are shown as well.

The difference computed by the comparison to independent geoid heights is composed by the following quantities:

$$\Delta N = h - H - (N + N^{HF}) \tag{3}$$

where

ΔN	=	Geoid difference
h	=	Ellipsoidal GNSS height
H	=	Height above local datum (normal height in case of Germany)
N	=	Geoid height (height anomaly in case of Germany) from GOCE model
N^{HF}	=	Geoid height (height anomaly) omission error from high frequency model and residual topography

So, all four quantities are contributing to total difference. In order to identify the contribution of N to the total sum one need to estimate the error levels of the other three quantities. Here the following uncertainties are assumed, which are estimated very conservative and at the lower level.

GNSS height error (σh):	1.0 cm
Sprit levelling error (σH):	1.0 cm
Residual omission error (σN^{HF})	0.5 cm

The total error of the geoid differences as shown in Figure 4-10 is given as:

DIR6/TIM6 differences $\sigma\Delta N$ at 105 km resolution:	1.8 cm
DIR6/TIM6 differences $\sigma\Delta N$ at 100 km resolution:	2.3 cm
TIM5 differences $\sigma\Delta N$ at 105 km resolution:	2.1 cm

Assuming that the different error levels as indicated above can be regarded as white noise errors, the error propagation law can be applied:

$$\sigma^2\Delta N = \sigma^2 h + \sigma^2 H + \sigma^2 N + \sigma^2 N^{HF} \tag{4}$$

By reversing the error propagation law finally one can estimate the model geoid errors applying the following formula:

$$\sigma N = \sqrt{\sigma^2\Delta N - \sigma^2 h - \sigma^2 H - \sigma^2 N^{HF}} \tag{5}$$

Applying equation (5) with the numbers provided above we get the following error estimates for the global model geoid at the chosen resolutions:

DIR6/TIM6 model error σN at 105 km resolution:	1.0 cm
DIR6/TIM6 model error σN at 100 km resolution:	1.7 cm
TIM5 model error σN at 105 km resolution:	1.5 cm

One can conclude from this empirical error analysis that the GOCE models have an accuracy of 1.0 cm at degree 190 and 1.7 cm at degree 200. This is well in-line with the mission goals which were defined as 1-2 cm at degree 200.

Finally, these geoid errors shall be compared to the estimated error maps computed from the full-variance-covariance matrices by error propagation up to degree and order 200, as shown in Figure 2-6, Figure 2-7 and Figure 2-8. From these figures we can extract the following geoid error in Germany:

DIR6 model error σN at 100 km resolution:	0.9 cm
TIM6 model error σN at 100 km resolution:	1.6 cm
TIM6e model error σN at 100 km resolution:	1.6 cm

From these analyses it can be assumed that the errors estimated by the TIM6 and TIM6e models are realistic and do not need to be calibrated, while the estimated errors of the DIR6 model need to be calibrated roughly by a factor of 1.8.

5. MODEL VALIDATION BY MEANS OF ORBIT TESTS

5.1 INTRODUCTION

This validation has been done for a selection of satellites with altitudes ranging from about 450 to about 6000 km. These satellites are ERS-2, CHAMP, GRACE-A/B and LAGEOS-1/2 for which a mature POD system was implemented (Gruber et al., 2011). The orbit computations are done with the NASA Goddard Space Flight Center (GSFC) GEODYN software (Pavlis et al., 2006). In fact, also POD tests were conducted for GOCE itself. For all cases, reference computations were done with the EIGEN-5S gravity field model (Förste et al., 2008).

The precise orbit determinations are based on different combinations of tracking data and on representative time periods (Table 5-1. Please note that the GOCE gravity field models were truncated at degree and order 200 (the full model was used if the associated maximum degree is lower than 200) for the POD of the CHAMP, GRACE and GOCE satellites. For the POD of the ERS-2 satellite, which flies at a significantly higher altitude, a maximum degree of 120 was applied. Finally, for the POD of the LAGEOS satellites, with an orbital altitude of about 5900 km, the gravity field models were truncated at degree and order 20.

Table 5-1: Tracking data types and periods for the selected satellites. The orbital arc lengths and the maximum spherical harmonic degree (lmax) used in the orbit determinations are indicated as well

ERS-2	- SLR, PRARE, Altimeter crossover observations - 7-day arcs - 2 January 1996 – 6 January 1997 (≈ 1 year) - $l_{max} = 120$
CHAMP	- GPS reduced-dynamic Cartesian coordinates - Accelerometer observations - Daily orbital arcs - 20-30 May 2001 - $l_{max} = 200$
GRACE-A/B	- GPS reduced-dynamic Cartesian coordinates - Accelerometer observations - Daily orbital arcs - 1-10 August 2002 - $l_{max} = 200$
LAGEOS-1/2	- SLR observations - 8-day arcs (1-day overlaps between consecutive arcs) - 5 January – 29 December 2002 (≈ 1 year) - $l_{max} = 20$
GOCE	- GPS kinematic Cartesian coordinates (RSO) - Common-mode accelerometer observations - Daily orbital arcs - 20-29 April 2010 - $l_{max} = 200$

5.2 RESULTS

The Root-Mean-Square (RMS of fit of ERS-2 Satellite Laser Ranging (SLR), Precise Range and Range-rate Equipment (PRARE) range (RNG) and Rage-rate (RR), single-satellite (SXO)

and ERS-2/TOPEX dual-satellite altimeter crossover (DXO) observations are included in Table 5-2.

Table 5-2: RMS-of-fit of tracking observations for ERS-2 with different gravity field models

Model	SLR (cm)	PRARE RNG (cm)	PRARE RR (mm/s)	SXO (cm)	DXO (cm)
EIGEN-5S	4.3	4.1	0.25	6.7	6.9
DIR6	4.3	4.2	0.25	6.8	6.9
TIM6	4.2	4.0	0.25	6.8	7.1
TIM6e	4.2	4.0	0.25	6.8	7.0

Altimeter crossover differences are averaged in geographical 2ox2o bins to reflect the mean (DXO) and ascending minus descending (SXO) geographically correlated radial orbit errors. The associated statistics are displayed in Table 5-3.

Table 5-3: RMS (cm) of geographically averaged ERS-2 single- (SXO) and ERS-2/TOPEX dual-satellite altimeter crossover (DXO) residuals with different gravity field models

	EIGEN-5S	DIR6	TIM6	TIM6e
SXO 2^ox2^o	2.1	2.3	2.3	2.3
DXO 2^ox2^o	1.9	2.5	2.5	2.5

For CHAMP and GRACE, the POD tests are done for 1-day orbital arcs. Fully dynamic POD for CHAMP is defined as the estimation of only 13 parameters: initial position (3) and velocity (3) at start time, 2 bias and scale factors for the accelerometer X and Y axes (4), and 3 empirical accelerations (one radial constant and one set of 1 cycle-per-orbital-revolution (cpr) radial sine/cosine coefficients) to account for the missing radial direction. For GRACE A and B, the same parameter set is estimated, except the 3 empirical accelerations are replaced by the additional bias and scale factor for the accelerometer Z axis (totaling 12 estimated parameters). The RMS-of-fit by this POD approach and setup of the coordinates from the reduced-dynamic orbit solutions is displayed in Table 5-4.

As a consistency test, also fully dynamic orbit determinations were conducted for GOCE, where the kinematic position coordinates from the Rapid Science Orbit (RSO) solution were used as observation, which have a precision of the order of 4 cm. The common-mode accelerations, which are produced by the gradiometer in addition to the gravity gradients, are a good representation of the (remaining) GOCE non-gravitational accelerations and are used in the POD, similar to the approach adopted for CHAMP and GRACE-A/B. Because of the drag-free control system, the non-gravitational accelerations are largely compensated and very small, which leads to very weakly observable scale factors. Therefore, the scale factors for the common-mode accelerations were kept equal to one and were not estimated. For GOCE, the estimated parameter set consisted of initial position and velocity (6 parameters) and 3 common-mode accelerometer biases (X, Y and Z direction), i.e. 9 parameters per 24-hr arc. The associated RMS-of-fit values are included in Table 5-4.

Table 5-4: RMS-of-fit of reduced-dynamic orbit solutions (CHAMP, GRACE) and kinematic orbit solutions (GOCE) for prior and GOCE gravity field models

Satellite	Model	X (cm)	Y (cm)	Z (cm)	3D (cm)
CHAMP	EIGEN-5S	24.2	17.9	28.5	41.4
	DIR6	24.6	18.3	28.9	42.1
	TIM6	26.6	22.1	29.7	45.5
	TIM6e	24.3	18.4	28.4	41.7
GRACE-A	EIGEN-5S	4.9	3.8	4.8	7.8
	DIR6	6.2	4.5	5.5	9.4
	TIM6	16.2	15.0	10.3	24.3
	TIM6e	9.6	5.7	7.7	13.6
GRACE-B	EIGEN-5S	4.8	3.7	4.6	7.6
	DIR6	5.8	4.3	5.2	8.9
	TIM6	14.9	14.9	9.4	23.1
	TIM6e	8.8	4.9	7.2	12.4
GOCE	EIGEN-5S	9.5	10.2	14.0	19.7
	DIR6	4.9	4.5	5.1	8.3
	TIM6	6.0	5.3	5.9	10.0
	TIM6e	5.9	5.2	5.8	9.8

Finally, orbits were recomputed with the selected gravity field models for the LAGEOS-1 and -2 satellites. The RMS-of-fit values of the SLR observations is displayed in Table 5-5.

Table 5-5: RMS-of-fit (cm) of SLR tracking observations for the LAGEOS satellites with different gravity field models.

	EIGEN-5S	DIR6	TIM6	TIM6e
LAGEOS-1	1.98	2.00	1.99	2.00
LAGEOS-2	1.80	1.83	1.82	1.83

6. SUMMARY

In summary the following conclusions can be drawn:

1. In a global average the GOCE rel. 6 models contain the full signal of the Earth gravity field up to degree and order 200 corresponding to 100 km spatial resolution.
2. With each release of the GOCE models (DIR and TIM series) the estimated coefficient errors were reduced.
3. With more data the errors decrease and more coefficients (with higher degrees) can be estimated with a signal to noise ratio better than 1. The rel. 6 models represent the ultimate solutions with highest possible signal and lowest error levels.
4. Oceanographic assessment shows that for MDT computations it is important to use GOCE between 250 and 400 km wavelengths, even in a combined geoid model.
5. Globally, the minimum quadratic mean of the difference with drifters filtered at wavelength 160km is reached for MDTs filtered at 250km. For this optimal wavelength, mean geostrophic currents estimated from release 6 GOCE models reach a ratio of noise versus signal smaller than 8% (25%) for the zonal (meridional) component.
6. GNSS-levelling geoid heights suffer from systematic problems mostly caused by the spirit levelling. Therefore, when comparing geoid heights from global models to GNSS-levelling geoid heights a planar correction surface needs to be applied.
7. Geoid differences to observed GNSS-Levelling geoid heights confirm that up to degree 200 all models, which are using GOCE information, perform significantly better.
8. The absolute accuracy of the rel. 6 GOCE models is estimated to 1.7 cm at 100 km resolution and 1.0 cm at 105 km resolution. This is determined by comparisons with the most recent German GNSS-Levelling data set, which is based on a complete resurvey with utmost precision.
9. The errors estimated by the TIM6 and TIM6e models are realistic and do not need to be calibrated, while the estimated errors of the DIR6 model need to be calibrated by roughly a factor of 1.8.
10. Orbit tests in general show slightly better performance for the DIR6 model than for the TIM6 model. This is caused by the combination of GOCE normal equations with those from the GRACE and Lageos missions.
11. The TIM6e model adding airborne, terrestrial and altimetric gravity data over the polar gap areas to the TIM6 model shows better performance for the orbit tests. Also the estimated geoid errors in the polar areas are significantly smaller.

Finally, it shall be stated that with the release 6 GOCE models the mission goals could be achieved and in some cases even be outperformed.

7. REFERENCES

Brockmann, J. M. 2014. “On High Performance Computing in Geodesy -- Applications in Global Gravity Field Determination.” Phd thesis, Bonn, Germany: Institute of Geodesy and Geoinformation, University of Bonn. http://nbn-resolving.de/urn:nbn:de:hbz:5n-38608.

Brockmann, J. M., N. Zehentner, E. Höck, R. Pail, I. Loth, T. Mayer-Gürr, and W.-D. Schuh. 2014. “EGM_TIM_RL05: An Independent Geoid with Centimeter Accuracy Purely Based on the GOCE Mission.” Geophysical Research Letters 41 (22): 8089–99. http://doi.org/10.1002/2014GL061904

Brockmann, Jan Martin; Schubert, Till; Mayer-Gürr, Torsten; Schuh, Wolf-Dieter (2019): The Earth's gravity field as seen by the GOCE satellite - an improved sixth release derived with the time-wise approach. GFZ Data Services. http://doi.org/10.5880/ICGEM.2019.003

Bruinsma S.L., Marty J.C., Balmino G., Biancale R., Foerste C., Abrikosov O. and Neumayer H, 2010, GOCE Gravity Field Recovery by Means of the Direct Numerical Method, presented at the ESA Living Planet Symposium, 27th June - 2nd July 2010, Bergen, Norway; See also: earth.esa.int/GOCE

Bruinsma, S., Förste, C., Abrikosov, O., Lemoine, J., Marty, J., Mulet, S., Rio, M. and Bonvalot, S. (2014): ESA's satellite-only gravity field model via the direct approach based on all GOCE data. - Geophysical Research Letters, 41, 21, pp. 7508-7514. DOI: http://doi.org/10.1002/2014GL062045

Dahle, C., Flechtner, F., Murböck, M., Michalak, G., Neumayer, K., Abrykosov, O., Reinhold, A., König, R.(2018): GRACE 327-743 (Gravity Recovery and Climate Experiment: GFZ Level-2 Processing Standards Document for Level-2 Product Release 06 (Rev. 1.0, October 26, 2018), (Scientific Technical Report STR - Data ; 18), GFZ German Research Centre for Geosciences : Potsdam, 20 p. DOI: http://doi.org/10.2312/GFZ.b103-18048

Förste, Christoph; Abrykosov, Oleh; Bruinsma, Sean; Dahle, Christoph; König, Rolf; Lemoine, Jean-Michel (2019): ESA's Release 6 GOCE gravity field model by means of the direct approach based on improved filtering of the reprocessed gradients of the entire mission. GFZ Data Services. http://doi.org/10.5880/ICGEM.2019.004

Förste C., Bruinsma S.L., Abrikosov O., Lemoine J.M., Marty J.C., Flechtner F., Balmino G., Barthelmes F. and R. Biancale, 2014, EIGEN-6C4 The latest combined global gravity field model including GOCE data up to degree and order 2190 of GFZ Potsdam and GRGS Toulouse. GFZ Data Services, http://doi.org/10.5880/icgem.2015.1

Förste, Ch., F. Flechtner, R. Schmidt, R. Stubenvoll, M. Rothacher, J. Kusche, H. Neumayer, R. Biancale, J.-M. Lemoine, F. Barthelmes, S. Bruinsma, R. Koenig and Ul. Meyer. (2008). EIGEN-GL05C - A new global combined high-resolution GRACE-based gravity field model of the GFZ-GRGS cooperation. Geophysical Research Abstracts, Vol. 10, EGU2008-A-03426, 2008 SRef-ID: 1607-7962/gra/EGU2008-A-03426, 2008.

Gruber, T.; Visser, P. N. A. M.; Ackermann, C.; Hosse, M. (2011): Validation of GOCE gravity field models by means of orbit residuals and geoid comparisons. Journal of Geodesy 85 (11), 2011, 845-860; https://doi.org/10.1007/s00190-011-0486-7

Gruber T., Rummel R., Abrikosov O. and van Hees R., 2014, GOCE Level 2 Product Data Handbook, Issue 5, European Space Agency, https://earth.esa.int/documents/10174/1650485/GOCE_Product_Data_Handbook_Level-2

Gruber, T.; Willberg, M. (2019): Signal and Error Assessment of GOCE-based High Resolution Gravity Field Models. Accepted for publication by Journal of Geodetic Science.

Hansen D.V., Poulain P.-M., (1996): Quality Control and Interpolations of WOCE-TOGA Drifter Data. J. Atmos. Oceanic Technol., 13, 900–909.

Hirt C., Kuhn M., Claessens S., Pail R., Seitz K. and Gruber T., 2014, Study of the Earth's short-scale gravity field using the ERTM2160 gravity model. Computers & Geosciences 73, 71-80, https://doi.org/10.1016/j.cageo.2014.09.001

Knudsen P., Andersen O., Maximenko N., Hafner J., 2019. A new combined mean dynamic topography model – DTUUH19MDT. Presented at Esa Living Planet 2019

Mayer-Gürr, T., K. H. Ilk, A. Eicker, and M. Feuchtinger. 2005. "ITG-CHAMP01: A CHAMP Gravity Field Model from Short Kinematic Arcs over a One-Year Observation Period." Journal of Geodesy 78 (7–8): 462–80. http://doi.org/10.1007/s00190-004-0413-2.

Mayer-Gürr T. and the GOCO Team, 2015, The combined satellite gravity field model GOCO05s, Geophysical Research Abstracts, Vol. 17, EGU2015-12364, EGU General Assembly 2015

Metzler B. and Pail R., 2005, GOCE Data Processing: The Sperical Cap Regularization Approach, Stud. Geophys. Geod. 49 (2005), 441-462

Pail R., Bruinsma S., Migliaccio F., Foerste C., Goiginger H., Schuh W.-D, Hoeck E, Reguzzoni M., Brockmann J.M, Abrikosov O., Veicherts M., Fecher T., Mayrhofer R., Krasbutter I., Sanso F. & Tscherning C.C., 2011, First GOCE gravity field models derived by three different approaches. Journal of Geodesy, 85, 11, 819-843

Pail, R.; Fecher, T.; Barnes, D.; Factor, J. F.; Holmes, S. A.; Gruber, T.; Zingerle, P.: Short note: the experimental geopotential model XGM2016. Journal of Geodesy 92 (4), 2018, 443—451, http://doi.org/10.1007/s00190-017-1070-6

Pavlis, D.E., Poulouse, S., McCarthy, J.J., (2006). GEODYN Operations Manual, Contractor report, SGT Inc., Greenbelt, MD.

Pujol, M.-I., Faugère, Y., Taburet, G., Dupuy, S., Pelloquin, C., Ablain, M., Picot, N., 2016. DUACS DT2014: the new multimission altimeter data set reprocessed over 20 years. Ocean Sci. 12, 1067–1090. https://doi.org/10.5194/os-12-1067-2016

Pujol I, Schaeffer P, Faugere Y, Raynal M, Dibarboure G, Picot N. (2018). Gauging the Improvement of Recent Mean Sea Surface Models: A New Approach for Identifying

and Quantifying Their Errors. Journal of Geophysical Research: Oceans. 20 https://doi.org/10.1029/2017JC013503

Rapp R.H., 1997, Use of potential coefficient models for geoid undulation determinations using a spherical harmonic representation of the height anomaly/geoid undulation difference, J Geod 71, 282–289, https://doi.org/10.1007/s001900050096

Rio, M.-H. and Hernandez, F., (2003): High-frequency response of wind-driven currents measured by drifting buoys and altimetry over the world ocean. Journal of Geophysical Research, 108(C8): 3283-3301.

Rio M.-H , S. Mulet and N. Picot, 2014. Beyond GOCE for the ocean circulation estimate: Synergetic use of altimetry, gravimetry and in-situ data provides new insight into geostrophic and Ekman currents. GRL.

Rio M.-H , S. Mulet H. Etienne, G. Dibarboure and N. Picot, 2019. The new CNES-CLS18 Global Mean Dynamic Topography. In preparation

Wang Y.M., Saleh J., Li X. and Roman D.R., 2012, The US Gravimetric Geoid of 2009 (USGG2009): model development and evaluation, J Geod, 86: 165, https://doi.org/10.1007/s00190-011-0506-7

Zingerle, Philipp; Brockmann, Jan Martin; Pail, Roland; Gruber, Thomas; Willberg, Martin (2019): The polar extended gravity field model TIM_R6e. GFZ Data Services. http://doi.org/10.5880/ICGEM.2019.005